Molecular Oncology

FEBS PRESS

PTEN-mediated dephosphorylation of 53BP1 confers cellular resistance to DNA damage in cancer cells

Jianfeng He[1], Caihu Huang[1], Yanmin Guo[1], Rong Deng[1], Lian Li[1], Ran Chen[1], Yanli Wang[1], Jian Huang[1], Junke Zheng[2], Xian Zhao[1] and Jianxiu Yu[1]

1 Department of Biochemistry and Molecular Cell Biology, Shanghai Key Laboratory of Tumor Microenvironment and Inflammation, Shanghai Jiao Tong University School of Medicine, China

2 Department of Pathophysiology, Key Laboratory of Cell Differentiation and Apoptosis of Chinese Ministry of Education, Shanghai Jiao Tong University School of Medicine, China

Keywords

53BP1; DNA damage repair; homologous recombination (HR) repair; PTEN; SUMOylation

Correspondence

J. Yu, Department of Biochemistry and Molecular Cell Biology, Shanghai Key Laboratory of Tumor Microenvironment and Inflammation, Shanghai Jiao Tong University School of Medicine, Shanghai 200025, China

E-mail: jianxiu.yu@shsmu.edu.cn; jianxiu.yu@gmail.com

Jianfeng He, Caihu Huang, Yanmin Guo and Rong Deng contributed equally to this article.

(Received 19 June 2023, revised 16 November 2023, accepted 5 December 2023, available online 12 December 2023)

doi:10.1002/1878-0261.13563

Homologous recombination (HR) repair for DNA double-strand breaks (DSBs) is critical for maintaining genome stability and conferring the resistance of tumor cells to chemotherapy. Nuclear PTEN which contains both phosphatidylinositol 3,4,5-trisphosphate 3-phosphatase and protein phosphatase plays a key role in HR repair, but the underlying mechanism remains largely elusive. We find that SUMOylated PTEN promotes HR repair but represses nonhomologous end joining (NHEJ) repair by directly dephosphorylating TP53-binding protein 1 (53BP1). During DNA damage responses (DDR), tumor suppressor ARF (p14ARF) was phosphorylated and then interacted efficiently with PTEN, thus promoting PTEN SUMOylation as an atypical SUMO E3 ligase. Interestingly, SUMOylated PTEN was subsequently recruited to the chromatin at DSB sites. This was because SUMO1 that was conjugated to PTEN was recognized and bound by the SUMO-interacting motif (SIM) of breast cancer type 1 susceptibility protein (BRCA1), which has been located to the core of 53BP1 foci on chromatin during S/G2 stage. Furthermore, these chromatin-loaded PTEN directly and specifically dephosphorylated phosphothreonine-543 (pT543) of 53BP1, resulting in the dissociation of the 53BP1 complex, which facilitated DNA end resection and ongoing HR repair. SUMOylation-site-mutated $PTEN^{K254R}$ mice also showed decreased DNA damage repair *in vivo*. Blocking the PTEN SUMOylation pathway with either a SUMOylation inhibitor or a p14ARF(2-13) peptide sensitized tumor cells to chemotherapy. Our study therefore provides a new mechanistic understanding of PTEN in HR repair and clinical intervention of chemoresistant tumors.

Abbreviations

△SIM5, deleted SIM5-1 and SIM5-2; 53BP1, TP53-binding protein 1; BRCA1, breast cancer type 1 susceptibility protein; Chro., chromatin; CPP-p14ARF(2-13), cell penetrating peptide fused by p14ARF(2-13aa); CPT, Camptothecin; DDR, DNA damage responses; DSBs, DNA double-strand breaks; DTT, dithiothreitol; EDTA, ethylenediamine tetraacetic acid; HE, Hematoxylin and Eosin; HR, homologous recombination; IHC, immunohistochemistry; IR, irradiation; IRIF, ionizing radiation-induced foci; MEFs, mouse embryonic fibroblasts; mSIMn, mutated amino acids of SIM into alanine; NHEJ, nonhomologous end joining; NT, nontreatment; p14ARF, tumor suppressor ARF; PTEN, phosphatase and tensin homolog deleted on chromosome ten; PTMs, post-translational modifications; RIF1, Rap1-interacting factor 1; RPA32, replication protein A 32 kDa subunit; Shieldin, a complex contain SHLD1, SHLD2, SHLD3 and REV7; SIM, SUMO-interacting motif; ssDNA, single-stranded DNA; WCL, whole-cell lysis; WT, wide type.

1. Introduction

DNA lesions caused by environmental or endogenous genotoxic insults are major threats to genomic integrity [1,2]. DNA double-strand breaks (DSBs) are the most deleterious DNA lesions, which cause gene mutation, cell death, development disorder, and tumor predisposition if not repaired correctly and promptly [3,4]. There are two major pathways for DSB repair, homologous recombination (HR), and nonhomologous end joining (NHEJ) repair [5]. 53BP1, a pro-choice of DSBs, promotes NHEJ repair through inhibiting recruitment of HR repair factors including BRCA1 and CtIP to DSB sites in G1 stage [6]. DNA damage-induced phosphorylation at multiple sites in the N terminus of 53BP1 mediates its interaction with downstream factors RIF1 and PTIP [7]. RIF1 recruits the Shieldin complex, of which the subunit SHLD2 directly binds ssDNA and blocks DNA end resection, and loss of this complex dramatically increases HR repair [8–10]. On the other hand, HR repair depends on the exist of sister chromatid, which occurs mainly in S/G2 stage. BRCA1, a critical regulator of HR repair, promotes multiple steps including DNA end resection, RAD51 loading and ssDNA strand pairing [11,12]. BRCA1 can recruit a ubiquitin E3 ligase UHRF1 to mediate polyubiquitination of RIF1, resulting in RIF1 dissociation from 53BP1 and thus promoting HR repair in S/G2 stage [13]. Moreover, BRCA1 can also facilitate dephosphorylation of 53BP1 during S/G2 stage [14]. The region coded by *exon11* of *BRCA1* is required for the dephosphorylation of 53BP1 and RIF1 release from DNA breaks; however, the underlying molecular mechanism remains largely elusive [15,16].

PTEN, a dual phosphatase, is frequently deleted, mutated or downregulated in a variety of human tumors [17]. In cytoplasm, PTEN antagonizes PI3K-AKT signaling through its lipid phosphatase activity, while loss of which markedly promotes tumor cell proliferation [17]. It has been well-documented that the nuclear PTEN plays a critical role in maintaining the genome stability, centrosome stability, replication stress recovery, and DSB repairs [18–24]. Post-translational modifications (PTMs) of PTEN including SUMOylation, phosphorylation, and methylation are involved in DNA damage and repair [18,21,24,25]. SUMOylation has been extensively studied in DNA damage repair [26,27], and many DNA damage response (DDR)-associated proteins including CtIP, BMI1, BLM, RAD52, and TOP2A can be induced occurring SUMOylation by replication stress, DSB and DNA crosslinking [28–33]. Especially, PTEN SUMOylation plays a key role in repairing for DSB, but the underlying mechanism remains unexplored. In addition, there still remains dispute about the function of PTEN protein phosphatase activity in DDR.

Here, we provided evidences that SUMOylation of PTEN was increased by SUMO-E3-like p14ARF in DDR. SUMOylated PTEN was recognized and then recruited by the N-terminal SUMO-interacting motif (SIM) of BRCA1 to the chromatin. PTEN located at chromatin directly and specifically dephosphorylated pT543 of 53BP1, leading to RIF1 release and therefore facilitating DNA end resection. PTEN^{K254R} knock-in mice model also showed HR deficiency in DDR *in vivo*. Notably, inhibiting SUMOylation of PTEN by either a SUMOylation inhibitor or a peptide p14ARF (2-13) sensitized tumor cells to DNA damage agents, which might provide a new therapeutic strategy for clinical intervention of chemo-resistant tumor cells.

2. Materials and methods

2.1. Cell culture, transfection and lentiviral infection

HEK293T (RRID: CVCL_0063), HEK293FT (RRID: CVCL_6911), DU145 (RRID: CVCL_0105), HeLa (RRID:CVCL_0030), H1299 (RRID:CVCL_B7N7), and mouse embryonic fibroblasts (MEFs) were cultured in DMEM supplemented with 10% FBS and 1% 100 U of penicillin, and 100 μg·mL^{-1} streptomycin (Yeasen, Shanghai, China). PC3 (RRID:CVCL_0035) was cultured in RPMI1640 supplemented with 10% FBS and 1% 100 U of penicillin, and 100 μg·mL^{-1} streptomycin (Yeasen). DU145-PTEN$^{-/-}$ was generated with CRSPR/Cas9. U2OS-DR-GFP was a gift from Dr Daming Gao [34]. *Pten*^{WT} and *Pten*^{K254R} MEFs were obtained from 13-day pregnant mouse embryos of wild-type and *Pten*^{K254R} knock-in C57BL/6 mice, respectively, and then immortalized with SV40-LT at passage three. The mice were purchased from BRL Medicine Company (Shanghai, China). The other cell lines were from Cell Bank/Stem Cell Bank, Chinese Academy of Sciences. All cell lines have been authenticated in the past 3 years by Short Tandem Repeat (STR) analysis. Experiments were performed in mycoplasma-free cells. Plasmids and siRNA transfection were carried out with PEI for HEK293T, HEK293T$^{Senp1-/-}$ and HEK293FT and Lipo2000 (Invitrogen, Carlsbad, CA, USA) for other cells following the manufacturer's protocol. Packaging lentiviral and subsequent infection of all cell lines were carried out according to protocol in our laboratory.

2.2. Antibodies, reagents, plasmids, siRNA, shRNA, and sgRNA

Antibodies used in this study were listed in Table S1. PTEN cDNA was subcloned into pCMV-Flag, pEF-5HA, pEGFP-C1, pCD510B, and pGEX-4T-1 vectors. shRNAs of BRCA1, PTEN and p14ARF were designed and cloned into the vector pLKO.1. RFP-PCNA was a gift from Prof Pumin Zhang [35]. Flag-53BP1 and Myc-BRCA1 were gifts form Prof Xingzhi Xu [36]. pCBASceI, EJ5-GFP, and DR-GFP were purchased from Addgene (Watertown, MA, USA). p14ARF was cloned into pGEX-4T-1, pEYFP-N1, and pCD513B vectors. PCR-mediated site-directed mutagenesis and truncated proteins were performed according to standard procedures to create the PTEN, p14ARF, 53BP1, and BRCA1 mutants. All clones were sequenced to confirm the desired mutations. siRNAs targeting BRCA1 were synthesized by GenePharma (Shanghai, China). Two sgRNAs were designed to knockout PTEN. In brief, sgRNA was insert into LentiCRISPR v2 and delivered into DU145 cells, each single clone was selected and cultured. PTEN knockout clones were identified and used in our study. A list of the sequence information for the shRNAs, siRNAs, and sgRNAs was provided in Table S2.

2.3. Immunoblot and denatured immunoprecipitation for SUMOylation detection

Cells were washed once with PBS and lysed in lysis buffer (50 mM Tris–HCl pH 7.4, 150 mM NaCl, 1 mM DTT, 1 mM EDTA, 1% NP-40, complete protease inhibitor cocktail (Roche, Basel, Switzerland) and 20 mM *N*-ethylmaleimide) on ice for 30 min, then lysates were sonicated and centrifuged at 12 000 ***g*** for 30 min. Protein concentrations were quantified with BCA kit (Thermo-Fisher, Waltham, MA, USA). Equivalent amounts of protein (1–2 mg) were incubated with 1 μg indicated antibody and 20 μL protein A/G beads (#IP05, Calbiochem, Oakville, Canada) at 4 °C overnight. Beads were collected with centrifugation and washed with lysis buffer for five times, and then boiled with 2× protein loading buffer before analysis by SDS/PAGE.

Denatured immunoprecipitation for SUMOylation detection was carried out as previously described with several modifications [37]. Briefly, cells were lysed with SUMO lysis buffer (62.5 mM Tris pH 6.8, 2% SDS), sonicated, and boiled after addition of 1 mM DTT. The lysis was centrifuged at 12 000 ***g*** for 15 min. Supernatant was transferred into new EP tube and diluted to a final concentration of 0.1% SDS with lysis buffer. Equivalent amounts of protein were incubated with indicated antibodies (anti-PTEN, anti-HA and anti-Flag) and protein A/G beads overnight at 4 °C. Beads were washed with lysis buffer containing 300 mM NaCl and 0.1% SDS for five times and boiled with 2× protein loading buffer before analysis by SDS/PAGE. All western blot experiments were repeated at least twice.

2.4. Ni^{2+}-NTA pull down for SUMOylation assay

For the detection of PTEN SUMOylation during DNA damage repair, 293T cells were transfected with His-SUMO1 and indicated plasmids for 48 h. CPT (#S1288, Selleck, Houston, TX, USA) and Zeocin (#60216ES80, Yeasen) were used to induce DNA damage for 1 h. cells were harvested at indicated time, 10% cells were used as input. SUMO-PTEN were pulled down with Ni^{2+}-NTA beads (#30210, Qiagen, Germantown, MD, USA) and analyzed with SDS/PAGE as previous described [25].

2.5. Immunofluorescence

Cells were seeded on glass coverslips. After treatment with various DNA damage stimuli, cells were washed with PBS and then fixed with 4% (w/v) paraformaldehyde in PBS for 15 min at room temperature. For immunofluorescence after pre-extraction, cells were treated with 1% triton/TBS for 5 min on ice before fixing. When staining RPA32, cells were pre-extracted with cold 0.5% Triton X-100 in PBS for 3 min before fixing. After fixing, cells were permeabilized with 0.5% (v/v) Triton X-100 in PBS for 60 min and blocked with 5% BSA in PBS for 60 min at room temperature. Generally, cells were then incubated with the primary antibody diluted in PBS-BSA overnight at 4 °C. Cells were washed three times with PBST and then incubated with secondary antibodies diluted in PBS-BSA supplemented with 2 $\mu g \cdot mL^{-1}$ of Hoechst 33342 (#62249, Thermo-Fisher) to stain DNA for 1 h at room temperature. Cells were washed three times with PBST and then the coverslips were mounted onto glass slides with Prolong Gold mounting agent (#P36931, Thermo-Fisher). Confocal images were taken with a LSM710 or Zeiss (Oberkochen, Germany) LSM880 laser-scanning confocal microscope.

For the discrimination of cells at S stage, cells were pre-incubated with 10 μM EdU (#C0081S, Beyotime, Shanghai, China) for 30 min before DNA damage induction. Click-It reaction were carried out as manufacture's protocol to staining EdU-positive cells. After this, cells were used for further immunostaining.

Intensity and number of DNA damage induced foci were counted with the FOCO software [38].

2.6. HR and NHEJ repair assay

To determine the efficiency of HR-mediated DSB repair in cells expressing different form of PTEN with mutation, we first generated stably PTEN knockdown U2OS-DR-GFP cells with shRNA. Then, PTEN-WT, C124S, G129E, K254R, and K266R were re-expressed in those cells. To increase RFP-I-Sce1 expression efficiency, RFP-I-Sce1 was subcloned into the vector CD510B. Pseudo-lentivirus expressing RFP-I-Sce1 was used to infect U2OS-DR-GFP cells. After 48–72 h, cells were collected for FACS analysis. Percentage of RFP- and GFP-positive cells were quantified. Homologous recombination efficiency was quantified as $(GFP^{+}/RFP^{+})*100\%$. For NHEJ repair efficiency, we first re-expressed PTEN-WT, C124S, G129E, K254R and K266R in U2OS-shPTEN cells. The NHEJ efficiency was detected with the EJ5-GFP reporter [39]. Plasmids EJ5-GFP and ISCE1-RFP were co-transfected into U2OS cells. Forty-eight hours after transfection, cells were collected and fixed for the flow cytometry analysis of RFP and GFP. The NHEJ efficiency was calculated by the ratio of GFP/RFP.

2.7. Laser micro-irradiation

Generation of localized DNA damage by laser was done as previously described [35]. Briefly, cells were seeded in a live-cell imaging culture dish, transfected with GFP-PTEN and RFP-PCNA and cultured for 48 h. 2 $\mu g \cdot mL^{-1}$ Hoechst 33342 was used to pre-sensitize cells for 10 min before laser micro-irradiation. For micro-irradiation, the cell dish was mounted on the stage of a Leica SP8 microscope at 37 °C. 405 nm UVA focused through a 63× 1.4NA oil objective was used to induce localized DNA damage. Laser power was set to 50% and iterations were set to 50 times. Time-lapse imaging of recruitment of GFP- or RFP-tagged proteins to DNA damage site was captured every 30 s after micro-irradiation with 488 and 561 nm laser.

2.8. GST pull-down

GST-fused protein was expressed in *Escherichia coli* BL21 and affinity-purified with GST beads (#17-0756-01, GE Healthcare Life Sciences, Marlborough, MA, USA). 293T cells overexpressing indicated proteins were treated with DNA damage reagents and lysed. And then cell lysates were incubated with above GST-fused protein beads overnight. Beads were collected and washed five times, followed by western blotting analysis.

2.9. *In vitro* dephosphorylation assay

For measuring dephosphorylation of 53BP1 by PTEN, the GST-fused $PTEN^{WT}$, $PTEN^{C124S}$, $PTEN^{G129E}$, and $PTEN^{G129R}$, as well as GST protein were purified from *E. coli* BL21. Full-length Flag-53BP1 and GFP-53BP1 were purified from 293T cells after Zeocin treatment. The dephosphorylation assays were performed in phosphatase assay buffer (20 $mmol \cdot L^{-1}$ HEPES, pH 7.2, 100 $mmol \cdot L^{-1}$ NaCl, and 3 $mmol \cdot L^{-1}$ DTT). The reactions were incubated at 37 °C for 60 min with or without the addition of recombinant GST-fused $PTEN^{WT}$, $PTEN^{C124S}$, $PTEN^{G129E}$, or $PTEN^{G129R}$, as well as GST protein as negative control, and then were stopped by adding 2× SDS loading buffer for immunoblotting analysis.

2.10. Cellular fractionation

Mouse embryonic fibroblasts, DU145, H1299 cells cultured with 90–100% confluence were harvested after treatment with DNA damage reagents and recovery for indicated time. Extraction of cytoplasmic and nuclear proteins was performed using the Nuclear/Cytosol Fractionation Kit (BioVision, Waltham, MA, USA) according to its instruction.

Separation of chromatin-associated proteins was performed as previously described with minor modification [40]. Briefly, cell pellets were washed with cold PBS and then incubated with buffer A (10 mM pH 7.9 HEPES, 10 mM KCl, 1.5 mM $MgCl_2$, 0.34 M sucrose, 10% glycerol, 1 mM DTT, protease inhibitors, 0.1% Triton-X100) for 10 min on ice. Cell pellets were collected with centrifugation and washed twice with buffer A. Next, cell pellets were gently resuspended in buffer B (3 mM EDTA, 0.2 mM EGTA, 1 mM DTT, protease inhibitors) and incubated for 30 min on ice. Then, cell pellets were collected by centrifugation and lysed in 2% SDS as chromatin-associated proteins. When detecting proteins tightly associated with chromatin, we pipetted cell pellets with buffer B harshly until sticky chromatin pellets were visible after incubation with buffer A. After another 30-min incubation in buffer B, chromatin pellets containing tightly associated proteins was collected by centrifugation and lysed with 2% SDS.

2.11. Cell viability and colony formation assay

For cell viability assay, cells were counted and 10 000 cells were seeded into 96-well plates. After 24 h, DNA

damage reagents were added and cultured for another 3 days. CCK8-kit was used to detect cell viability and all quantitative results were normalized to non-treatment group. For colony formation assay, 500 or 1000 cells were seeded into a 12-well plate. After 24 h, CPT and Zeocin were added for 48 h and replaced with fresh medium. Cisplatin was added into medium for 72 h and replaced with fresh medium. All culture medium was changed every 3 days until colony was visible. Colonies were washed, fixed and stained with 0.1% crystal violet overnight. Visible colonies were counted and analyzed between groups with IMAGEJ.

2.12. Cell cycle profile and EdU incorporation assay

Cells were collected and fixed by 4% PFA when proliferated to 80–90% in culture dish. DNA content and cell cycle profile was determined by flow cytometry after PI staining. The EdU incorporation assay was performed to detect cell proliferation rate. EdU (10 μM) was added into culture dish for 2 h when cell proliferated to 80–90% and then fixed with 4% PFA. Click-It reaction were carried out as manufacture's protocol to staining EdU positive cells. After this, percentage of EdU-positive cells were quantified by flow cytometry.

2.13. Mouse model and IHC

All animal studies were conducted with the approval and guidance of Shanghai Jiao Tong University Medical Animal Ethics Committees (Approval NO. A-2019-036). The mice were housed in specific pathogen-free environment, handled with care, and allowed for adaption to the environment before experiments. *Pten*-K254R and *Pten*-K266R knockin C57BL/6 mice were generated by BRL medicine company with CRISPR-Cas9 and homozygous mice were verified with PCR sequencing. For IHC, 4-month-old male mice were chosen and subjected to whole body irradiation (IR) with 8 Gy. Mice were sacrificed at Day 4 post IR, small intestines were used for histological analysis. HE staining were used to quantify villi length, and Ki67 staining was used to identify proliferating cells in small intestines.

2.14. Statistical analysis

Group data are presented as mean with or without ± SD. The statistical significance between experimental groups was determined by Student's *t*-test (two tailed and unpaired). $P < 0.05$ was considered to be significant (n.s., not significant; $*0.01 < P < 0.05$, $**0.001 < P < 0.01$ and $***P < 0.001$). If not specified, analysis was performed with GRAPHPAD PRISM 8 (Boston, MA, USA).

2.15. Ethics approval

All procedures followed were in accordance with the ethical standards of the Animal Care and Use Committee of School of medicine, Shanghai Jiao Tong University. All institutional and national guidelines for the care and use of laboratory animals were followed.

3. Results

3.1. PTEN promotes HR repair through facilitating DNA end resection

We first validated the role of PTEN in DSB repair. As shown in Fig. S1A–C, knockdown of PTEN in DU145 cells indeed delayed DSB repair after the treatment with Zeocin (a radiomimetic reagent), as measured by ionizing radiation-induced foci (IRIF) of γH2AX and 53BP1 [18,24]. Either PTEN knockdown in DU145 and HeLa cells or PTEN knockout in MEFs reduced the numbers of RAD51 (a key HR repair regulator) foci (Fig. S1D–F), which was consistent with previous reports [18,21]. In addition to RAD51 filament formation, DNA end resection, a key step prior to RAD51, is also critical for the choice of DSB repair pathway and can be regulated in many ways [41]. To test whether PTEN regulates DNA end resection, we detected the phosphorylation level of RPA32(S4/8), a surrogate marker of ssDNA accumulation and DNA end resection [42], to show that knockdown of PTEN downregulated pS4/8-RPA32 in HeLa cells after irradiation (IR) treatment (Fig. 1A), suggesting that PTEN is involved in the regulation of DNA end resection in DSB repair.

To further identify whether both the phosphatase activity and SUMOylation of PTEN are required for its role in DNA end resection, we used the CRISPR/Cas9 system to knockout PTEN in DU145 cells and then stably re-expressed $PTEN^{WT}$, $PTEN^{C124S}$ (dual phosphatase dead), $PTEN^{G129E}$ (lipid phosphatase dead, but protein phosphatase still active), $PTEN^{K254R}$ (SUMO-site mutant) and $PTEN^{K266R}$ (SUMO-site mutant) (Fig. S1G). As expectedly, knockout of PTEN decreased IR-induced pS4/8-RPA32 in DU145 cells (Fig. 1B). There were little differences on pS4/8-RPA32 among $PTEN^{WT}$, $PTEN^{C124S}$ and $PTEN^{G129E}$ after IR treatment; however, pS4/8-RPA32 was decreased in $PTEN^{K254R}$ and $PTEN^{K266R}$ compared to that in

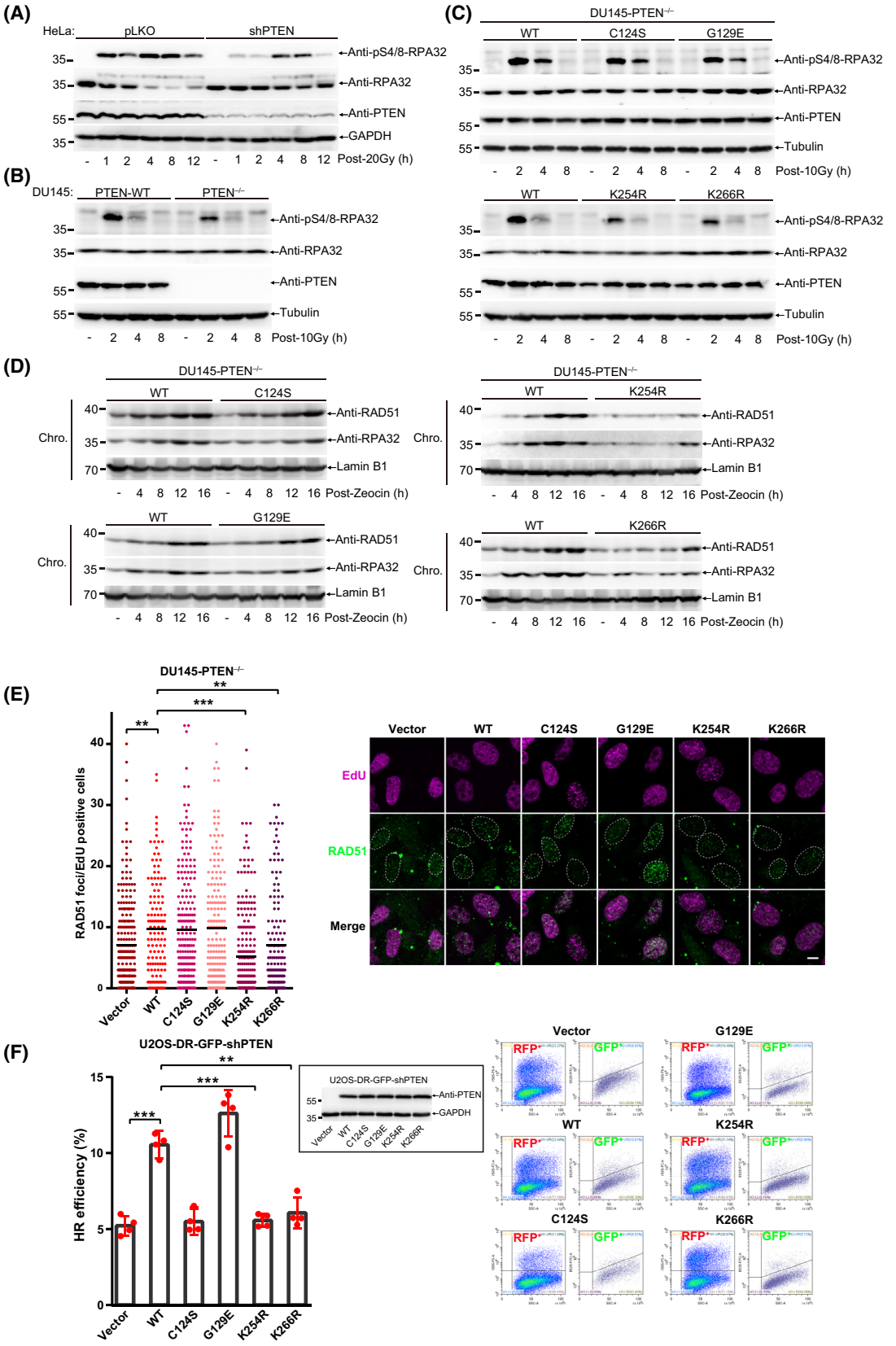
(A)
HeLa:
pLKO
shPTEN
Anti-pS4/8-RPA32
Anti-RPA32
Anti-PTEN
GAPDH
Post-20Gy (h)
(B)
DU145:
PTEN-WT
PTEN-/-
Anti-pS4/8-RPA32
Anti-RPA32
Anti-PTEN
Tubulin
Post-10Gy (h)
(C)
DU145-PTEN-/-
WT
C124S
G129E
K254R
K266R
Anti-pS4/8-RPA32
Anti-RPA32
Anti-PTEN
Tubulin
Post-10Gy (h)
(D)
DU145-PTEN-/-
Chro.
Anti-RAD51
Anti-RPA32
Lamin B1
Post-Zeocin (h)
(E)
DU145-PTEN-/-
RAD51 foci/EdU positive cells
Vector
WT
C124S
G129E
K254R
K266R
EdU
RAD51
Merge
(F)
U2OS-DR-GFP-shPTEN
HR efficiency (%)
Anti-PTEN
GAPDH
RFP
GFP

Fig. 1. PTEN promotes HR repair through facilitating DNA end resection. (A) Immunoblot of pS4/8-RPA32 of HeLa-pLKO and -shPTEN cells treated with 20 Gy and recovery for indicated time. (B) Immunoblot of pS4/8-RPA32 of DU145-PTEN^{WT} and -PTEN$^{-/-}$ cells treated with 10 Gy and recovered for indicated time. (C) Immunoblot of pS4/8-RPA32 of DU145-PTEN$^{-/-}$ cells stably re-expressed PTEN$^{WT,\ K254R}$ and ^{K266R} cells after treated with 10 Gy. (D) Immunoblot of chromatin associated RPA32 and RAD51 in DU145 cells after treated with Zeocin (200 μg·mL^{-1}) for 1 h and recovered for indicated time. (E) RAD51 foci were quantified in DU145 cells treated with 5 Gy and recovery for 6 h and then presented with dot graph. Representative images of RAD51 foci were shown at right panel. scale bar, 20 μm. (F) HR (homologous recombiantion) efficiency were detected in U2OS-DR-GFP-shPTEN cells stably re-expressing PTEN^{WT}, PTEN^{C124S}, PTEN^{G129E}, PTEN^{K254R} and PTEN^{K266R}. Inset: immunoblot of PTEN in U2OS-DR-GFP-shPTEN cells stably re-expressing indicated PTEN mutants. Left panel: quantification of HR efficiency shown as bar graph. Right panel: representative images of FACS. Unpaired Student's *t*-test was used (**$P < 0.01$, ***$P < 0.001$) and data were shown as mean or mean ± SD. All results were shown with one representative image from three independent experiments. Chro., chromatin; FACS, fluorescence-activated cell sorting; HR, homologous recombination; WT, wide type.

PTEN^{WT} (Fig. 1C). Similar results of PTEN^{K254R} and PTEN^{K266R} in decreasing pS4/8-RPA32 were also observed by using other DNA damage reagents including Zeocin and Camptothecin (CPT) in DU145 (Fig. S1H,I), and IR in PC3 cells (Fig. S1J). Thus, above results suggest that SUMOylation but not phosphatase activity of PTEN is associated with DNA end resection.

Determination of chromatin-associated proteins has been often applied to monitor DNA damage repair process, for examples, chromatin loading of RPA32 and RAD51 can represent HR efficiency [21,40,43,44]. When compared with PTEN^{WT}, mutants PTEN^{K254R} and PTEN^{K266R} inhibited the chromatin loading of RPA32 and RAD51 in DU145 cells induced by Zeocin (Fig. 1D), Etoposide (Fig. S1K) and CPT (Fig. S1L), whereas PTEN^{C124S} and PTEN^{G129E} seemed not affect (Fig. 1D). We also detected chromatin associated p-RPA32 with immunofluorescence after pre-extraction in DU145 cells and the results were consistent with western blot results (Fig. S1N). Furthermore, we also investigated IRIF of RAD51 in S phase (EdU^{+}) cells to show the similar pattern of results that numbers of RAD51 foci were comparable among PTEN^{C124S}, PTEN^{G129E} and PTEN^{WT}, but decreased in PTEN^{K254R} and PTEN^{K266R} (Fig. 1E). These results suggest that SUMOylation but not phosphatase activity of PTEN affects the chromatin loading of RPA32 and RAD51.

In addition to RAD51 foci as a marker of HR repair, an HR reporter of DR-GFP was employed to detect the overall efficiency of HR repair [45]. In accordance with previous reports, HR efficiency was reduced after PTEN knockdown (Fig. S1M). Surprisingly, HR efficiency was also compromised in PTEN^{C124S}, as like PTEN^{K254R} and PTEN^{K266R}, but not in PTEN^{G129E}, suggesting PTEN protein phosphatase was indispensable for it function in HR repair efficiency despite its little influence on chromatin loading of RPA32 and RAD51 (Fig. 1F). We also detected the NHEJ repair efficiency of these mutants with EJ5-GFP reporter [39]. Knockdown of PTEN and re-expressing PTEN^{WT} or mutants in U2OS cells did not change the NHEJ repair efficiency (Fig. S1O,P). Given cell cycle can regulate the choice of DNA damage repair pathway, we detected cell cycle profile and EdU incorporation in different human cancer cell lines used in this study. There is no obvious difference in cell cycle among parental, PTEN knockdown, PTEN knockout and PTEN reconstituted cells of HeLa and DU145 (Fig. S1R,S). We only observed a mild decrease of S phase cell population when overexpressing PTEN in PC3 cells, which might be due to downregulation of PI3K/AKT signaling (Fig. S1Q). There was no significant difference in percentage of EdU incorporation in HeLa, PC3, and reconstituted DU145-PTEN$^{-/-}$ cells (Fig. S1T–V). In summary, considering that HR repair mainly occurs in the S/G2 phase, the above results demonstrated that the difference in HR repair efficiency in these cells was not due to the influence of cell cycle or cell proliferation. Taken together, these data provide substantial evidences that PTEN promotes HR repair partially through enhancing DNA end resection, which is dramatically abolished when its SUMO-sites mutated.

3.2. DNA damage promotes PTEN chromatin loading by inducing its SUMOylation

As previous reported [29], DNA damage stimuli can strongly induce SUMOylation of proteins involved in different DNA damage repair pathways. To further investigate the induction and turnover of PTEN SUMO modification in DNA damage repair, we overexpressed His-SUMO1 and Flag-PTEN in 293T cells. After Zeocin treatment, cells were collected and lysed at different recovery time as indicated, and His-SUMO1 modified proteins were enriched with Ni^{2+}-NTA agarose beads (Fig. 2A) and Co-IP (Fig. S2A) methods under denatured condition. Interestingly, SUMOylated PTEN was significantly increased

overtime by Zeocin treatment. Similarly, CPT treatment also enhanced SUMOylation of PTEN (Fig. 2B). These data strongly demonstrated that DNA damage stimuli promoted PTEN SUMOylation. To further determine which SUMO-site is responsible for SUMO1 conjugation induced by DNA damage and whether its phosphatase activity is involved in this process, we overexpressed His-SUMO1 and Flag-tagged $PTEN^{C124S}$, $PTEN^{G129E}$, $PTEN^{K254R}$ or $PTEN^{K266R}$ in 293T cells and detected SUMOylated PTEN with the method of Ni^{2+}-NTA agarose pull down. In contrast to mutations C124S and G129E, both mutations of K254R and K266R led to significant reduction of PTEN SUMOylation induced by Zeocin, suggesting that these two SUMO-sites were critical for DDR (Fig. 2C).

One previous study reported that K254R mutation prevented PTEN nuclear localization and DNA damage repair function in U87MG glioblastoma cells [18], however our results of immunofluorescence showed no changes in the localization between $PTEN^{WT}$ and $PTEN^{K254R}$ or $PTEN^{K266R}$ in DU145 cells under normal condition (Fig. 2D). We also observed there was little effects on PTEN nuclear localization in DU145 cells after IR treatment (Fig. S2C). Consistently, the detection of the nuclear PTEN level in non-treated and IR-treated DU145 cells with nuclear-cytosol fractionation showed the same result that IR treatment had no effect on PTEN nuclear localization (Fig. S2D). Furthermore, we detected the influence of IR on subcellular localization of PTEN in DU145-shPTEN-$PTEN^{WT/K254R/K266R}$ cells with immunofluorescence. After IR treatment, there was still no difference in PTEN localization between $PTEN^{WT}$, mutant $PTEN^{K254R}$, and $PTEN^{K266R}$ (Fig. S2E). Moreover, another two nuclear-cytosol separation results also revealed that the localizations of PTEN were almost not affected in DU145-$PTEN^{-/-}$ re-expressing PTEN-WT and mutants including $PTEN^{K254R}$, $PTEN^{K266R}$, $PTEN^{C124S}$, and $PTEN^{G129E}$ cells even after treatments with Zeocin (Fig. 2E) and CPT (Fig. S2B). More interestingly, the nuclear location of $PTEN^{C124S}$ was markedly higher than that of all others (Fig. 2E and Fig. S2B), the underlying mechanism should be further studied. Although SUMO-site mutations K254R and K266R had little influence on PTEN nuclear localization, we wanted to assess whether SUMOylation of PTEN influences its chromatin loading under DNA damage. First, we observed that PTEN was indeed recruited into the DNA-damage location induced by the laser micro-irradiation (Fig. S2F). Second, Zeocin (Fig. 2F) and CPT (Fig. S2G) treatments induced PTEN accumulation on the chromatin. The chromatin loading of $PTEN^{K254R}$ was significantly suppressed whereas that of $PTEN^{G129E}$ and $PTEN^{K266R}$ was similar with $PTEN^{WT}$ after Zeocin and CPT treatments. For the case of $PTEN^{K266R}$, it was unexpectedly and might be a different mechanism from $PTEN^{K254R}$. In accordance with enhanced nuclear localization of PTEN-C124S, the chromatin loading of $PTEN^{C124S}$ was remarkably increased (Fig. 2F), but how the mutation C124S to increase the nuclear localization and chromatin loading of PTEN was not clear. Third, to further validate whether SUMOylated PTEN can directly accumulate on the chromatin, we separated chromatin associated proteins under harsh condition. After IR treatment, one shifted band with higher molecular weight than normal PTEN was clearly observed in re-expression of $PTEN^{WT}$ but not SUMO-site mutants $PTEN^{K254R}$ and $PTEN^{K266R}$ in DU145-$PTEN^{-/-}$ cells (Fig. 2G). Given that endogenous *PTEN* gene in DU145 cells was knocked out with CRSPR/Cas9 technique, this shift band from re-expression of normal $PTEN^{WT}$ was most likely to be SUMOylated-PTEN other than variants of PTEN such as PTEN α or β isoform.

Collectively, all above results demonstrate that DNA damage promotes PTEN SUMOylation and

Fig. 2. DNA damage promotes PTEN chromatin loading by inducing its SUMOylation. (A) 293T cells transfected with His-SUMO1 and Flag-PTEN were treated with Zeocin (200 $\mu g \cdot mL^{-1}$) for 1 h and recovered for indicated time. His-SUMO1 conjugates were pulled down with Ni^{2+}-NTA beads and SUMOylated PTEN were analyzed with immunoblot. (B) 293T cells transfected with His-SUMO1 and Flag-PTEN were treated with CPT (20 μM) for 1 h and recovered for indicated time. His-SUMO1 conjugates were pulled down with Ni^{2+}-NTA beads and SUMOylated PTEN were analyzed with immunoblot. (C) 293T cells transfected with His-SUMO1 and Flag-$PTEN^{WT,\ C124S,\ G129E,\ K254R,\ K266R}$ were treated with Zeocin (200 $\mu g \cdot mL^{-1}$) for 1 h and recovered for 4 h, Ni^{2+}-NTA pulldown were used to analyze PTEN SUMOylation. (D) Images of staining of PTEN in DU145-shPTEN cells stably re-expressed PTEN-WT, K254R and K266R. scale bar, 20 μm. (E) Nuclear(N)-Cytosol(C) separation was performed in DU145-$PTEN^{-/-}$ cells stably re-expressing $PTEN^{WT,\ C124S,\ G129E,\ K254R}$ and ^{K266R} treated with Zeocin (400 $\mu g \cdot mL^{-1}$) for 1 h and recovery for 4 h. Localization of PTEN was detected with immunoblot. (F) Immunoblot of chromatin associated PTEN in DU145 cells treated with Zeocin (400 $\mu g \cdot mL^{-1}$) for 1 h and recovery for indicated time. (G) Chromatin protein separation were performed at harsh condition in DU145-$PTEN^{-/-}$ cells stably re-expressing $PTEN^{WT,\ K254R}$ and ^{K266R} after treatment with 10 Gy. PTEN tightly associated with chromatin was detected with immunoblot. All results were shown with one representative image from three independent experiments. Chro., chromatin; CPT, camptothecin; WT, wide type.

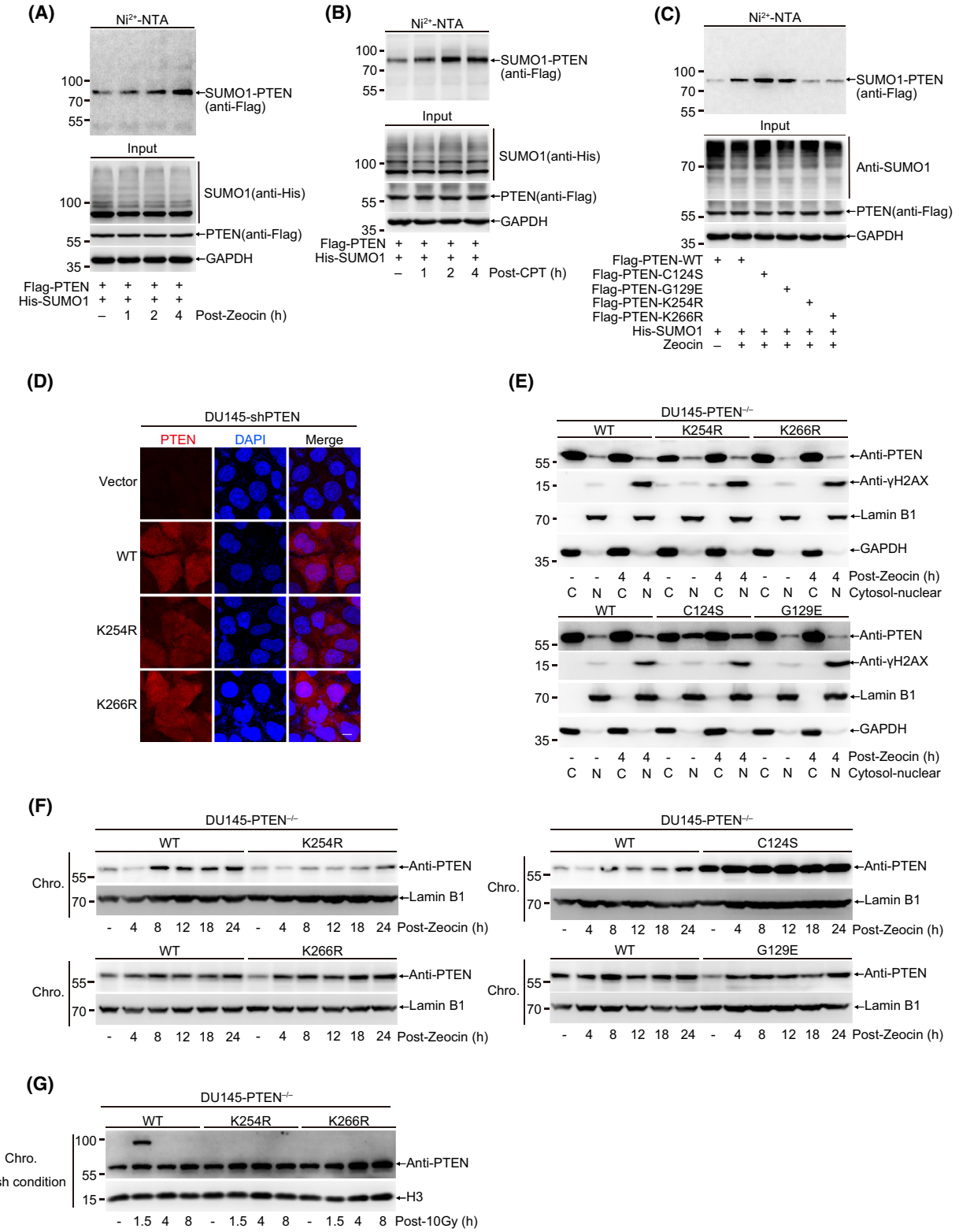
(A)
Ni2+-NTA
100
70
55
SUMO1-PTEN (anti-Flag)
Input
100
SUMO1(anti-His)
55
PTEN(anti-Flag)
35
GAPDH
Flag-PTEN + + + +
His-SUMO1 + + + +
– 1 2 4 Post-Zeocin (h)
(B)
Ni2+-NTA
100
70
55
SUMO1-PTEN (anti-Flag)
Input
100
SUMO1(anti-His)
55
PTEN(anti-Flag)
35
GAPDH
Flag-PTEN + + + +
His-SUMO1 + + + +
– 1 2 4 Post-CPT (h)
(C)
Ni2+-NTA
100
70
55
SUMO1-PTEN (anti-Flag)
Input
70
Anti-SUMO1
55
PTEN(anti-Flag)
35
GAPDH
Flag-PTEN-WT + +
Flag-PTEN-C124S +
Flag-PTEN-G129E +
Flag-PTEN-K254R +
Flag-PTEN-K266R +
His-SUMO1 + + + + + +
Zeocin – + + + + +
(D)
DU145-shPTEN
PTEN DAPI Merge
Vector
WT
K254R
K266R
(E)
DU145-PTEN-/-
WT K254R K266R
55
15
70
35
Anti-PTEN
Anti-γH2AX
Lamin B1
GAPDH
- - 4 4 - - 4 4 - - 4 4 Post-Zeocin (h)
C N C N C N C N C N C N Cytosol-nuclear
WT C124S G129E
55
15
70
35
Anti-PTEN
Anti-γH2AX
Lamin B1
GAPDH
- - 4 4 - - 4 4 - - 4 4 Post-Zeocin (h)
C N C N C N C N C N C N Cytosol-nuclear
(F)
DU145-PTEN-/-
WT K254R
Chro.
55
70
Anti-PTEN
Lamin B1
- 4 8 12 18 24 - 4 8 12 18 24 Post-Zeocin (h)
WT K266R
Chro.
55
70
Anti-PTEN
Lamin B1
- 4 8 12 18 24 - 4 8 12 18 24 Post-Zeocin (h)
DU145-PTEN-/-
WT C124S
Chro.
55
70
Anti-PTEN
Lamin B1
- 4 8 12 18 24 - 4 8 12 18 24 Post-Zeocin (h)
WT G129E
Chro.
55
70
Anti-PTEN
Lamin B1
- 4 8 12 18 24 - 4 8 12 18 24 Post-Zeocin (h)
(G)
DU145-PTEN-/-
WT K254R K266R
Chro.
harsh condition
100
55
15
Anti-PTEN
H3
- 1.5 4 8 - 1.5 4 8 - 1.5 4 8 Post-10Gy (h)

especially K254-SUMOylation of PTEN is essential for its chromatin loading.

3.3. p14ARF is a novel SUMO E3 ligase to mediate PTEN SUMOylation during DDR

p14ARF, a well-known tumor suppressor, is an atypical SUMO E3 ligase for promoting SUMOylation of its binding proteins such as MDM2, NPM, and EGR1 [37,46,47]. Interestingly, we found that PTEN SUMOylation was dramatically enhanced by overexpression of p14ARF and UBC9 (SUMO-conjugating enzyme E2) (Fig. 3A and Fig. S3A) whereas suppressed by knockdown of p14ARF (Fig. 3B). Since p14ARF promotes SUMOylation of target proteins via direct interaction, we assumed p14ARF might interact with PTEN. Co-IP and GST-pull down results showed that p14ARF directly bound to PTEN in cells and *in vitro* (Fig. 3C,D and Fig. S3B). To identify the interaction region between p14ARF and PTEN, we generated a series of truncates (Fig. S3C) and performed co-IP. Two regions of 2-14aa and 82-101aa in p14ARF are important for substrate interaction, and deletion of these two regions dramatically inhibit SUMO conjugation on substrates mediated by p14ARF [48]. Our results also showed that these two regions in p14ARF were required for their interaction. Deletion of either one reduced their interaction and deletion of both completely abolish their interaction (Fig. 3E and Fig. S3D,E). Moreover, the ability of p14ARF to enhance PTEN SUMOylation was indeed weakened when deletion of either one region. Although both regions contributed to PTEN SUMOylation, p14ARF(Δ2–14) seemed to be more effective than p14ARF(Δ82–101) in suppression of PTEN SUMOylation (Fig. 3F). In addition, we identified that the C-terminal region 188-403aa of PTEN mediated its interaction with p14ARF (Fig. S3F).

Since DNA damage stimuli can induce PTEN SUMOylation, we wondered whether p14ARF is involved in this process. Knockdown of p14ARF substantially reduced Zeocin-induced PTEN SUMOylation (Fig. 3G). In response to treatments with both Zeocin (Fig. 3H) and CPT (Fig. S3G), the interaction between exogenous PTEN and p14ARF was obviously enhanced. CPT treatment also significantly increased the interaction between endogenous PTEN and p14ARF in DU145 cells (Fig. S3H). Given that phosphorylation signal is critical for DDR and there is exactly one threonine (T8) located in p14ARF(2-14aa), which can be phosphorylated [49], so we detected the phosphorylation of p14ARF with the method of Phos-tag gel and showed a clear shifted band of p14ARF, which was increased after Zeocin treatment (Fig. 3I), suggesting that DNA damage induced phosphorylation of p14ARF. The mutation T8A at p14ARF significantly inhibited the interaction between PTEN and p14ARF, on the contrary, the mutation T8D enhanced their interaction not only under normal condition but also after treatment with CPT (Fig. 3J). The mutation T8A of p14ARF also attenuated its ability to promote PTEN SUMOylation after Zeocin treatment (Fig. 3K). Consistently, knockdown of p14ARF inhibited PTEN chromatin loading while overexpression of p14ARF increased its loading (Fig. 3L and Fig. S3I–K). Knockdown of p14ARF also sensitized DU145 cell to

Fig. 3. p14ARF is a novel SUMO E3 ligase to mediate PTEN SUMOylation during DDR. (A) 293T cells were transfected with His-SUMO1, HA-UBC9, Myc-p14ARF and Flag-PTEN for 48 h. His-SUMO1 conjugates were pulled down with Ni^{2+}-NTA beads and SUMOylated PTEN were analyzed with immunoblot. (B) 293T-pLKO or shARF-1 cells were transfected with His-SUMO1, HA-UBC9 and Flag-PTEN for 48 h. His-SUMO1 conjugates were pulled down with Ni^{2+}-NTA beads and SUMOylated PTEN were analyzed with immunoblot. (C) 293T cells were transfected with Myc-p14ARF and Flag-PTEN for 48 h. Co-IP were used to detect interaction between PTEN and p14ARF. (D) GST pull-down were used to detect interaction between PTEN and p14ARF. Upper panel: GST-PTEN was purified from BL21 and incubated with 293T lysis which transfected with HA-p14ARF for 48 h. Lower panel: GST-p14ARF was purified from BL21 and incubated with 293T lysis which transfected with Flag-PTEN for 48 h. (E) Truncated Myc-p14ARF and Flag-PTEN were transfected into 293T cells, interaction domain between PTEN and p14ARF were identified with Co-IP. (F) Truncated Myc-p14ARF, His-SUMO1, Flag-UBC9 and HA-PTEN were transfected into 293T cells. His-SUMO1 conjugates were pulled down with Ni^{2+}-NTA beads and SUMOylated PTEN were analyzed with immunoblot. (G) His-SUMO1 and HA-PTEN were transfected into 293T-pLKO and shARF-1 cells. After 48 h, cells were treated with Zeocin (400 $\mu g \cdot mL^{-1}$) for 1 h and recovery for indicated time. His-SUMO1 conjugates were pulled down with Ni^{2+}-NTA beads and SUMOylated PTEN were analyzed with immunoblot. (H) Interaction between PTEN and p14ARF post CPT (20 μM) treatment were detected with Co-IP in 293T cells. (I) Phosphorylation of p14ARF after Zeocin (400 $\mu g \cdot mL^{-1}$) treatment for 1 h and recovery for indicated time was detected with phos-tag gel. (J) Interaction of PTEN and p14ARF-WT, T8A and T8D were detected under normal condition or CPT (20 μM) treatment with Co-IP in 293T cells. (K) 293T cells were transfected with Flag-SUMO1, Myc-p14ARF-WT or T8A and HA-PTEN for 48 h. Flag-SUMO1 conjugates were immunoprecipitated and SUMOylated PTEN were analyzed with immunoblot. (L) chromatin loading of PTEN were detected with immunoblot in DU145-pLKO and shARF-1 cells after treatment with CPT (20 μM) for 1 h and recovery for indicated time. All results were shown with one representative image from three independent experiments. Chro., chromatin; Co-IP, Co-immunoprecipitation; CPT, camptothecin; GST, glutathione S-transferase tag; WCL, whole cell lysis; WT, wide type.

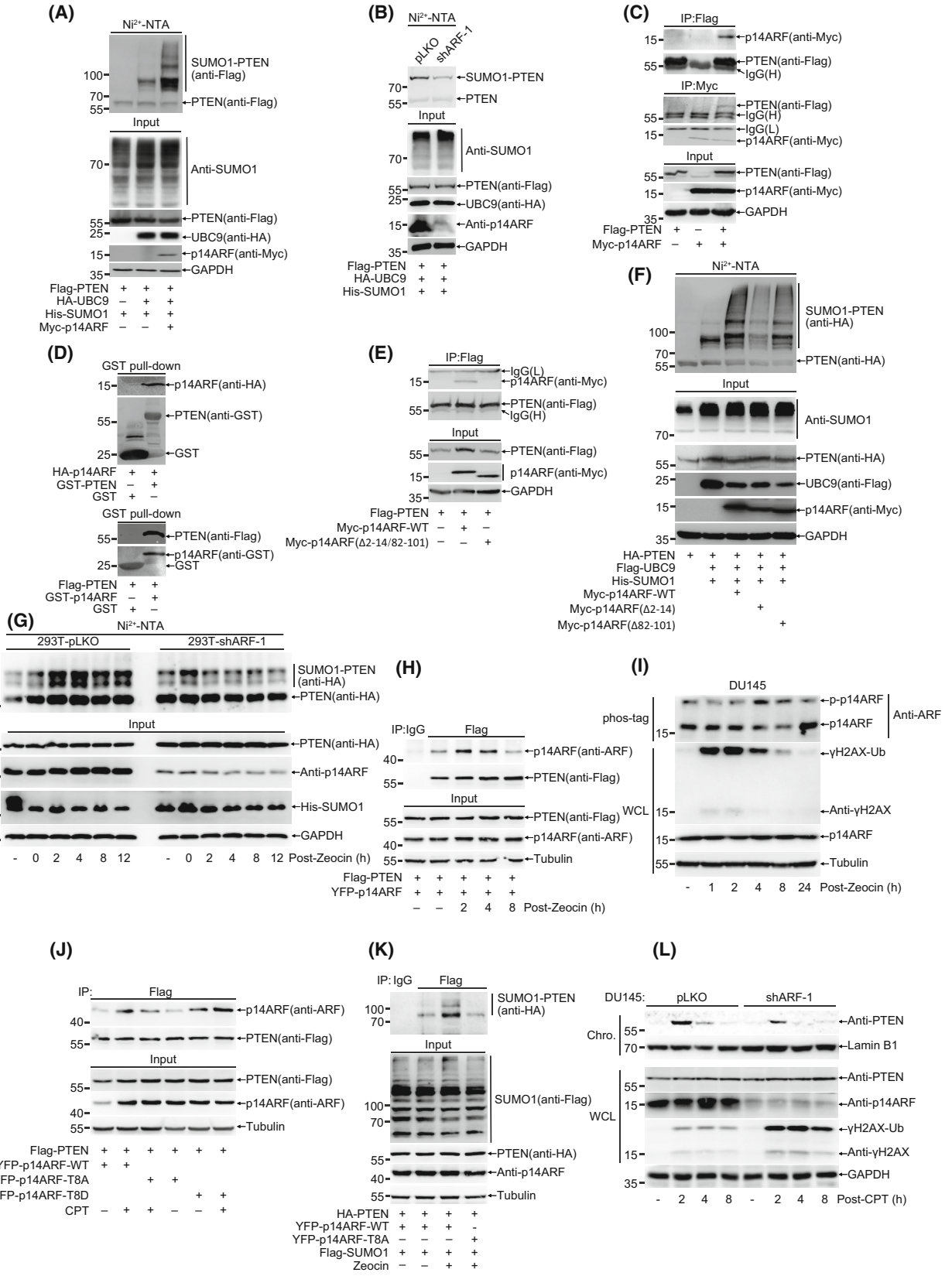
(A)
Ni2+-NTA
SUMO1-PTEN (anti-Flag)
PTEN(anti-Flag)
Input
Anti-SUMO1
PTEN(anti-Flag)
UBC9(anti-HA)
p14ARF(anti-Myc)
GAPDH
Flag-PTEN
HA-UBC9
His-SUMO1
Myc-p14ARF
(B)
Ni2+-NTA
pLKO
shARF-1
SUMO1-PTEN
PTEN
Input
Anti-SUMO1
PTEN(anti-Flag)
UBC9(anti-HA)
Anti-p14ARF
GAPDH
Flag-PTEN
HA-UBC9
His-SUMO1
(C)
IP:Flag
p14ARF(anti-Myc)
PTEN(anti-Flag)
IgG(H)
IP:Myc
PTEN(anti-Flag)
IgG(H)
IgG(L)
p14ARF(anti-Myc)
Input
PTEN(anti-Flag)
p14ARF(anti-Myc)
GAPDH
Flag-PTEN
Myc-p14ARF
(D)
GST pull-down
p14ARF(anti-HA)
PTEN(anti-GST)
GST
HA-p14ARF
GST-PTEN
GST
GST pull-down
PTEN(anti-Flag)
p14ARF(anti-GST)
GST
Flag-PTEN
GST-p14ARF
GST
(E)
IP:Flag
IgG(L)
p14ARF(anti-Myc)
PTEN(anti-Flag)
IgG(H)
Input
PTEN(anti-Flag)
p14ARF(anti-Myc)
GAPDH
Flag-PTEN
Myc-p14ARF-WT
Myc-p14ARF(Δ2-14/82-101)
(F)
Ni2+-NTA
SUMO1-PTEN (anti-HA)
PTEN(anti-HA)
Input
Anti-SUMO1
PTEN(anti-HA)
UBC9(anti-Flag)
p14ARF(anti-Myc)
GAPDH
HA-PTEN
Flag-UBC9
His-SUMO1
Myc-p14ARF-WT
Myc-p14ARF(Δ2-14)
Myc-p14ARF(Δ82-101)
(G)
Ni2+-NTA
293T-pLKO
293T-shARF-1
SUMO1-PTEN (anti-HA)
PTEN(anti-HA)
Input
PTEN(anti-HA)
Anti-p14ARF
His-SUMO1
GAPDH
- 0 2 4 8 12 - 0 2 4 8 12 Post-Zeocin (h)
(H)
IP:IgG Flag
p14ARF(anti-ARF)
PTEN(anti-Flag)
Input
PTEN(anti-Flag)
p14ARF(anti-ARF)
Tubulin
Flag-PTEN
YFP-p14ARF
– – 2 4 8 Post-Zeocin (h)
(I)
DU145
phos-tag
p-p14ARF
p14ARF
Anti-ARF
γH2AX-Ub
WCL
Anti-γH2AX
p14ARF
Tubulin
- 1 2 4 8 24 Post-Zeocin (h)
(J)
IP: Flag
p14ARF(anti-ARF)
PTEN(anti-Flag)
Input
PTEN(anti-Flag)
p14ARF(anti-ARF)
Tubulin
Flag-PTEN
YFP-p14ARF-WT
YFP-p14ARF-T8A
YFP-p14ARF-T8D
CPT
(K)
IP: IgG Flag
SUMO1-PTEN (anti-HA)
Input
SUMO1(anti-Flag)
PTEN(anti-HA)
Anti-p14ARF
Tubulin
HA-PTEN
YFP-p14ARF-WT
YFP-p14ARF-T8A
Flag-SUMO1
Zeocin
(L)
DU145: pLKO shARF-1
Chro.
Anti-PTEN
Lamin B1
WCL
Anti-PTEN
Anti-p14ARF
γH2AX-Ub
Anti-γH2AX
GAPDH
- 2 4 8 - 2 4 8 Post-CPT (h)

Cisplatin (Fig. S3L). All these results suggest that p14ARF is a functional SUMO E3 ligase responsible for promoting SUMOylation of PTEN during DDR.

3.4. PTEN relieves HR repair barrier posted by 53BP1 through directly dephosphorylating pT543-53BP1

Given that HR repair efficiency is compromised when PTEN lacking protein phosphatase activity [18] (Fig. 1F), next we tried to identify potential protein substrates targeted by PTEN in DNA damage repair. 53BP1, a key negative regulator of HR repair, is phosphorylated at multiple S/TQ sites which are essential for recruitment of downstream effectors [7]. Thus, we first examined the phosphorylation levels of 53BP1 in cells after treatment with CPT or Zeocin. The pT543-53BP1, which is necessary for recruitment of RIF1, was dramatically increased in PTEN-knockdown DU145 and HeLa cells (Fig. 4A, left panels) whereas significantly decreased in PTEN overexpression in PC3 cells which are devoid of endogenous PTEN (Fig. 4A, right and upper panel) after treatment with CPT (for 30 min). Moreover, we also detected the pT543-53BP1 level in PTEN-knockout DU145 cells after treatment with higher concentration of CPT for 1 h, to show that the pT543-53BP1 level was higher and lasted longer in PTEN-knockout cells than that of PTEN-WT cells (Fig. 4A, right and lower panel). Consistent with above results, when treated with Zeocin, the pT543-53BP1 level was increased in PTEN-knockdown DU145 and HeLa cells (Fig. S4A), while weakened in PTEN overexpression in PC3 cells (Fig. S4B). In addition, we confirm that the intensity of pT543-53BP1 foci was stronger in PTEN-knockdown DU145 than control cells (Fig. 4B and Fig. S4C) by staining with antibody pT543-53BP1.

Since it has been reported that PTEN loss led to the increase of pS25/29-53BP1 after treatment with etoposide and the mutation S25A enhanced RIF1 recruitment during DNA damage repair [24,50]; thus, we also detected the dynamics of pS25/29-53BP1 in PTEN-knockdown or -knockout cells after treatment with CPT or Zeocin. Indeed, pS25/29-53BP1 was induced in both PTEN-WT and PTEN-knockout DU145 cells after treatment with CPT. Increased pS25/29-53BP1 level was the same and even a little down whereas as expectedly, increased pT543-53BP1 level was higher in PTEN-knockout DU145 when compared with PTEN-WT DU145 (Fig. 4C). Furthermore, after treatment with Zeocin, the number and intensity of pT543-53BP1 foci were expectedly increased in DU145-shPTEN cells compared to those in DU145-pLKO cells (Fig. 4D); in contrast, there was little difference in the number and intensity of pS25-53BP1 foci between DU145-pLKO and DU145-shPTEN cells (Fig. 4E). These results demonstrate that PTEN regulates the level of pT543-53BP1 other than pS25/29-53BP1 in DDR.

As pT543-53BP1 helps to recruit RIF1 to DNA breaks [7], so we stained RIF1 in DU145-pLKO and shPTEN cells after IR treatment. In accordance with the pT543-53BP1 levels, the number and intensity of RIF1 foci were both increased (Fig. 4F). It has been well-documented that the 53BP1-RIF1-shieldin axis forms a barrier to inhibit HR repair through suppressing DNA end resection and HR repair mainly occurs at S/G2 of cell cycle [9,10,51,52], we wondered that whether PTEN in regulation of pT543-53BP1 is dependent on cell cycle. DU145 cells were firstly synchronized at G1/S with double thymidine block, and then directly released 5 h to enter S phase or synchronized at G1 with lovastatin, respectively. Cyclin A2 was used to show synchronization efficiency (Fig. S4D). The pT543-53BP1 levels were enhanced in both G1 and S

Fig. 4. PTEN relieves HR barrier posted by 53BP1 through directly dephosphorylating pT543-53BP1. (A) Immunoblot of pT543-53BP1 in DU145 (top left), HeLa (lower left) cells and PC3 (top right) after treatment with CPT (2 μM) for 30 min and recovery for indicated time. pT543-53BP1 was also detected in DU145 (lower right) cells after treated with CPT (20 μM) for 1 h and recovery for indicated time. (B) Dot graph of pT543-53BP1 foci intensity in DU145 cells after Zeocin (100 $\mu g \cdot mL^{-1}$) treatment for 30 min and recovery for indicated time. (C) Immunoblot of pT543-53BP1 and pS25/29-53BP1 in DU145 cells after treatment with CPT (20 μM) for 1 h and recovery for indicated time. (D) Dot graph of pT543-53BP1 foci number and intensity after Zeocin (200 $\mu g \cdot mL^{-1}$) treatment for 1 h and recovery for 2 h. Representative images were shown at right panel. scale bar, 20 μm. (E) Dot graph of pS25-53BP1 foci number and intensity after Zeocin (200 $\mu g \cdot mL^{-1}$) treatment for 1 h and recovery for 2 h. Representative images were shown at right panel. scale bar, 20 μm. (F) Dot graph of RIF1 foci number and intensity after Zeocin (200 $\mu g \cdot mL^{-1}$) treatment for 1 h and recovery for 2 h. Representative images were shown at right panel. scale bar, 20 μm. (G) Immunoblot analysis of pT543-53BP1 level in DU145-PTEN$^{-/-}$ cells stably re-expressed PTEN-WT, C124S and G129E after 10 Gy treatment and recovery for indicated time. (H) Dot graph of pT543-53BP1 foci number and intensity in DU145-PTEN$^{-/-}$ cells stably re-expressed PTEN-WT, C124S and G129E after 5 Gy treatment and recovery for 2 h. (I) *in vitro* phosphatase assay. GFP tagged phosphorylated 53BP1(1–600) were purified from 293T cells. GST-PTEN^{WT}, ^{C124S} and ^{G129E} were purified from *E. coli* BL21. Unpaired Student's *t*-test was used (**$P < 0.01$, ***$P < 0.001$) and data were shown as mean. *n.s.*, not significant. All results were shown with one representative image from three independent experiments. CPT, camptothecin; GST, glutathione S-transferase tag; NC, negative control; WT, wide type.

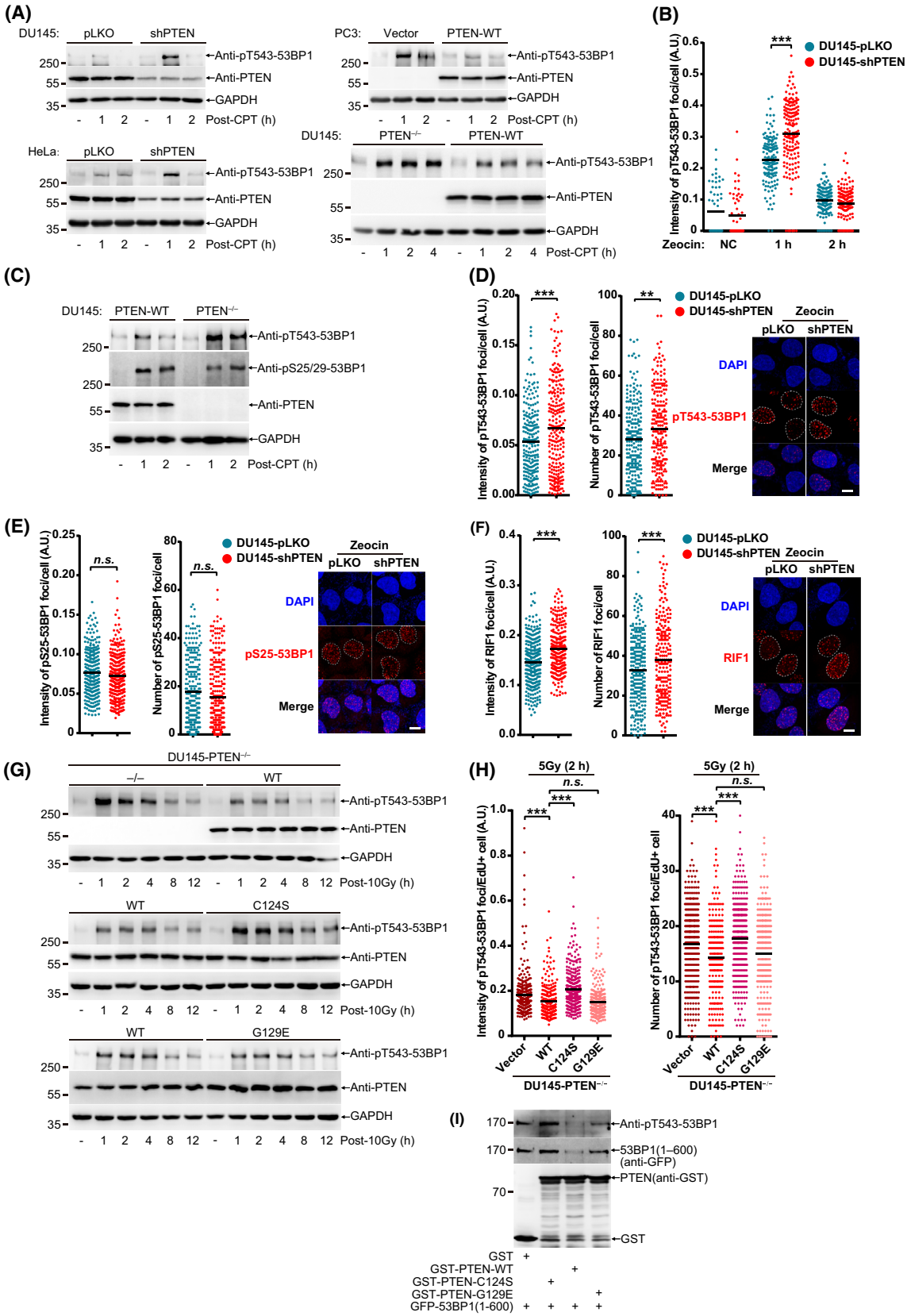
(A)
DU145: pLKO shPTEN
PC3: Vector PTEN-WT
HeLa: pLKO shPTEN
DU145: PTEN-/- PTEN-WT
Anti-pT543-53BP1
Anti-PTEN
GAPDH
Post-CPT (h)
(B)
DU145-pLKO
DU145-shPTEN
Intensity of pT543-53BP1 foci/cell (A.U.)
Zeocin: NC 1 h 2 h
(C)
DU145: PTEN-WT PTEN-/-
Anti-pS25/29-53BP1
(D)
Intensity of pT543-53BP1 foci/cell (A.U.)
Number of pT543-53BP1 foci/cell
Zeocin
pLKO shPTEN
DAPI
pT543-53BP1
Merge
(E)
Intensity of pS25-53BP1 foci/cell (A.U.)
Number of pS25-53BP1 foci/cell
n.s.
pS25-53BP1
(F)
Intensity of RIF1 foci/cell (A.U.)
Number of RIF1 foci/cell
RIF1
(G)
DU145-PTEN-/-
-/- WT
WT C124S
WT G129E
Post-10Gy (h)
(H)
5Gy (2 h)
Intensity of pT543-53BP1 foci/EdU+ cell (A.U.)
Number of pT543-53BP1 foci/EdU+ cell
Vector WT C124S G129E
DU145-PTEN-/-
(I)
Anti-pT543-53BP1
53BP1(1–600) (anti-GFP)
PTEN(anti-GST)
GST
GST
GST-PTEN-WT
GST-PTEN-C124S
GST-PTEN-G129E
GFP-53BP1(1-600)

phases after treatment with Zeocin (Fig. S4E,F). However, the increased pT543-53BP1 levels in S phase were much weaker in $PTEN^{WT}$ cells than those $PTEN^{-/-}$ cells (Fig. S4E). In contrast, the increased pT543-53BP1 levels in G1 phase were slightly weaker in $PTEN^{WT}$ cells when compared with $PTEN^{-/-}$ cells (Fig. S4F). These data suggest that PTEN regulating pT543-53BP1 is a cell-cycle dependent manner and mainly occurs in S phase.

To further verify whether PTEN phosphatase is responsible for dephosphorylating pT543-53BP1, we determined the pT543-53BP1 levels in $PTEN^{-/-}$, $PTEN^{WT}$, $PTEN^{C124S}$ and $PTEN^{G129E}$ DU145 cells. After treatment with IR or Zeocin, the pT543-53BP1 levels in $PTEN^{-/-}$ cells were higher than those in $PTEN^{WT}$ cells, as was expected (Fig. 4G and Fig. S4G, top panels). We found that pT543-53BP1 was increased in $PTEN^{C124S}$ but not in $PTEN^{G129E}$ cells when compared with $PTEN^{WT}$ cells (Fig. 4G and Fig. S4G, middle and low panels). As similar to immunoblot results, the number and intensity of pT543-53BP1 foci were also increased in $PTEN^{C124S}$ but not in $PTEN^{G129E}$ cells compared to those in $PTEN^{WT}$ DU145 cells at 2 h after treatment with IR (5 Gy) (Fig. 4H and Fig. S4H). Above results indicated that PTEN protein phosphatase was required for dephosphorylation of pT543-53BP1. Thus, we further speculated whether PTEN directly dephosphorylates pT543-53BP1.

To verify above hypothesis, we first purified phosphorylated full-length Flag-53BP1 from 293T cells for the *in vitro* reaction with GST-$PTEN^{WT}$ or GST-$PTEN^{G129R}$ (a dual phosphatase deficient mutant). The following western blotting results showed that PTEN-WT but not PTEN-G129R efficiently dephosphorylated pT543-53BP1 (Fig. S4I), suggesting that the PTEN phosphatase activity is required for dephosphorylation of pT543-53BP1. However, we noticed that Flag-53BP1 partly degraded after the *in vitro* reaction with GST-$PTEN^{WT}$ other than GST-$PTEN^{G129R}$. Given that 53BP1 consists of 1972 aa which is a relatively high-molecular-weight protein and could be much easier degraded when purified for *in vitro* reaction, we constructed a short truncated form, GFP-53BP1(1–600), for *in vitro* phosphatase assay. We found that GFP-53BP1(1–600) was easily detected by antibody anti-pT543-53BP1 and more strongly after CPT treatment; on the contrary, GFP-53BP1(1–300) could not be detected (Fig. S4J), suggesting this antibody could still specifically recognize phosphorylated T543 in GFP-53BP1(1–600). In order to further distinguish protein phosphatase and lipid phosphatase of PTEN in dephosphorylation of pT543-53BP1, similarly, we purified phosphorylated GFP-53BP1(1–600) from 293T cells for the *in vitro* reaction with GST-$PTEN^{WT}$, GST-$PTEN^{C124S}$ or GST-$PTEN^{G129E}$. Consistent with cellular results, $PTEN^{C124S}$ lost the ability to dephosphorylate pT543-53BP1, whereas $PTEN^{G129E}$ could moderately dephosphorylate pT543-53BP1 but was less efficient than PTEN-WT, which might be because the G129E mutation not only abolished lipid phosphatase of PTEN, but also reduced its protein phosphatase by about a half [53] (Fig. 4I). However, we still noticed that GFP-53BP1(1–600) partly degraded after the *in vitro* reaction with GST-$PTEN^{WT}$ and GST-$PTEN^{G129E}$, but not GST-$PTEN^{C124S}$, suggesting that phosphorylation modification might be important to maintain 53BP1 protein stability *in vitro*. Thus, above results suggest that PTEN directly dephosphorylates pT543-53BP1 *in vitro* and in DDR.

Taken together, our data demonstrate that PTEN directly dephosphorylates pT543-53BP1 in response to DNA damage, which relieves HR repair barrier posted by 53BP1.

3.5. PTEN chromatin loading is mediated by BRCA1 recruiting SUMOylated PTEN via its N-terminal SIM

BRCA1 can remove HR repair barrier posted by 53BP1 via several molecular mechanisms, including

Fig. 5. PTEN chromatin loading is mediated by BRCA1 recruiting SUMOylated PTEN via its N-terminal SIM. (A) Immunoblot of pT543-53BP1 in DU145 cells in which BRCA1 were knockdown with siControl or siBRCA1-1 after Zeocin (400 $\mu g \cdot mL^{-1}$) treatment for 1 h and recovery for indicated time. (B) Immunoblot of chromatin loaded PTEN and pS4/8-RPA32 in BRCA1 knockdown DU145 cells after treatment with CPT (20 μM) for 1 h and recovery for indicated time. (C) $293T^{senp1-/-}$ cells were transfected with Myc-BRCA1, HA-UBC9, His-SUMO1 and Flag-PTEN for 48 h. Co-IP were performed to identify interaction between PTEN and BRCA1. (D) $293T^{senp1-/-}$ cells were transfected with Myc-BRCA1, HA-UBC9, His-SUMO1 and Flag-PTEN (WT or mutants) for 48 h and treated with Zeocin. Co-IP were performed to identify interaction between PTEN (WT or mutants) and BRCA1. (E) $293T^{senp1-/-}$ cells were transfected with Myc-BRCA1(WT or SIM mutants), HA-UBC9, His-SUMO1 and Flag-PTEN for 48 h. Co-IP were performed to identify interaction between PTEN and BRCA1 (WT or SIM mutants). (F) Immunoblot of pT543-53BP1 in DU145-$PTEN^{-/-}$ cells stably re-expressed PTEN-WT, K254R and K266R after treatment with Zeocin (400 $\mu g \cdot mL^{-1}$) for 1 h and recovery for indicated time. All results were shown with one representative image from three independent experiments. Chro., chromatin; CPT, camptothecin; WCL, whole cell lysis; WT, wide type.

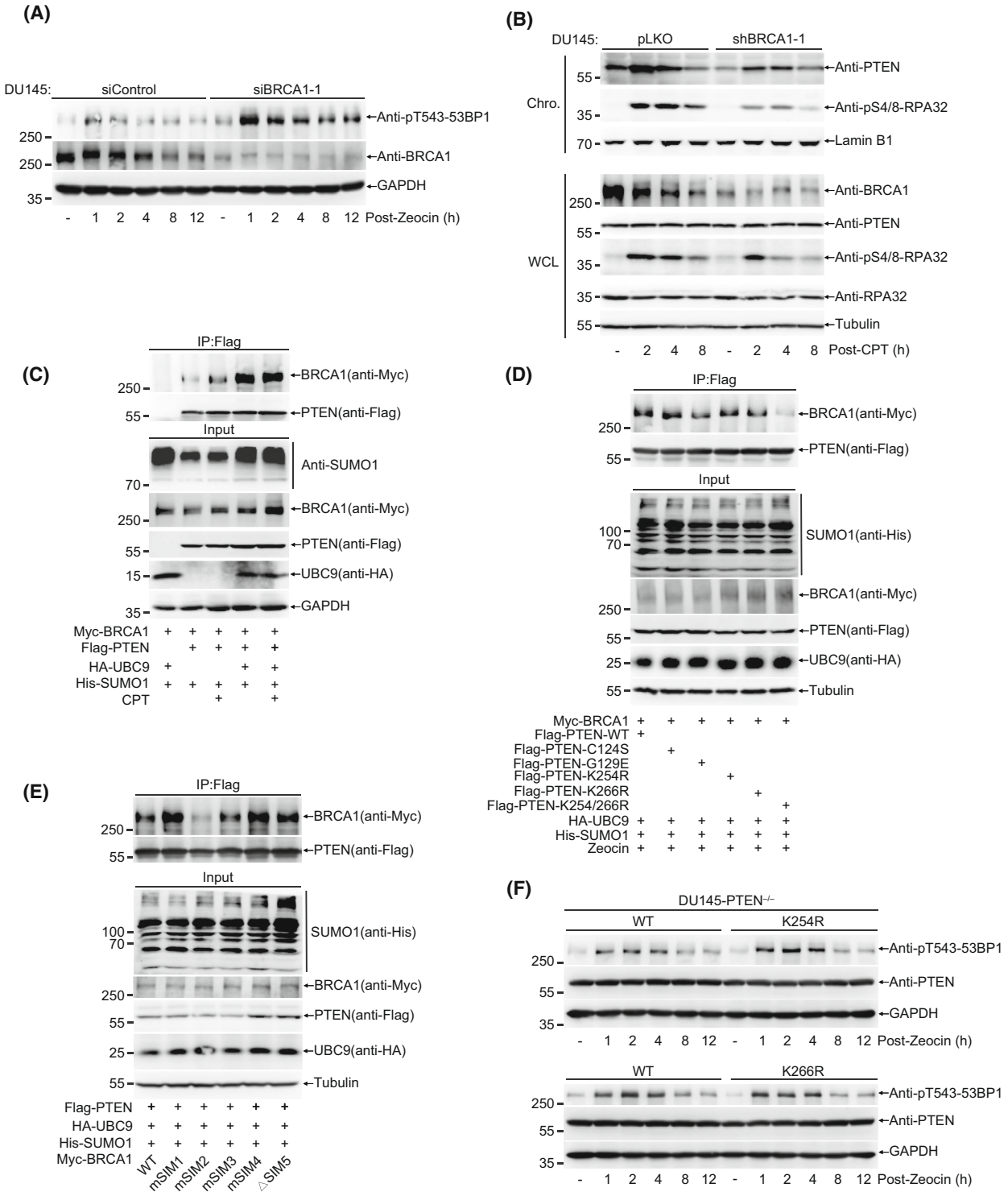

suppression of 53BP1 phosphorylation induced by DNA damage [14], so we wondered whether PTEN is a downstream effector of BRCA1. As expectedly, knockdown of BRCA1 by siRNA strongly increased the pT543-53BP1 level in DU145 after Zeocin treatment (Fig. 5A). Consistent with this, knockdown of BRCA1 by either siRNA or shRNA displayed the same results of enhancing pT543-53BP1 in U2OS cells after treatment with Zeocin and Etoposide (Fig. S5A). For the other hand, we questioned whether BRCA1 is

involved in PTEN chromatin loading. Indeed, chromatin separation experiments showed that knockdown of BRCA1 by shRNA or siRNA significantly suppressed PTEN chromatin loading as well as pS4/8-RPA32 (as a positive control) in DU145 cells after treatment with CPT, indicating that BRCA1 was needed for PTEN chromatin loading during DDR (Fig. 5B and Fig. S5B). Therefore, we next tested whether PTEN interacts with BRCA1 and this can be enhanced by SUMOylation. We transfected Flag-PTEN and Myc-BRCA1 with SUMO1 into *Senp1*$^{-/-}$ (SUMO Specific Peptidase 1) 293T cells for 48 h, and then treated with or without CPT. Co-IP/western blotting results showed that PTEN interacted with BRCA1, and the interaction was moderately enhanced by CPT treatment. Most strikingly, the interaction was strongest when cotransfected with SUMO1 and UBC9, which was not increased any more even with CPT treatment (Fig. 5C). Furthermore, CPT greatly increased the interaction between endogenous PTEN and BRCA1 in DU145 cells (Fig. S5C). To identify whether the interaction is specifically enhanced by SUMO1 modification, we also detected the ability of other SUMO isoform SUMO2 whose amino acid sequence is a little different from SUMO1. The interaction was much weaker in SUMO2 transfected than that in SUMO1 transfected cells under CPT treatment. Surprisingly, cotransfected with SUMO2 and UBC9 did not enhance the interaction at all (Fig. S5D). These data suggest that the interaction between PTEN and BRCA1 is specifically promoted by SUMO1 modification.

Given that the SUMO-site mutation of PTEN inhibited its chromatin loading induced by DNA damage, we wondered whether the interaction between PTEN and BRCA1 is directly mediated by SUMO-SIM (SUMO interacting motif), which is an important mechanism to mediate the protein–protein interaction. Indeed, the double mutations K254/266R of PTEN remarkably repressed the interaction although the single mutation K254R or K266R did not inhibit, suggesting SUMO1 modification of PTEN was important for its interaction with BRCA1. Additionally, the lack of lipid phosphatase activity of mutants PTEN^{C124S} and PTEN^{G129E} did not affect the interaction (Fig. 5D).

To identify SIMs of BRCA1 which are responsible for the interaction with SUMO1 attached to PTEN, we used two software GPS-SUMO and JASSA [54,55] to predict possible SIMs of BRCA1 (Fig. S5E,F). Since depletion of *exon11* of BRCA1 abolishes its suppression on 53BP1 phosphorylation and DNA end resection [15,16], we mainly focused on SIMs located in this region, which are marked in red (Fig. S5E,F). Further to find out which SIM is essential for the interaction, we mutated amino acids of SIM1, 2, 3, 4, into alanine, referred as mSIMn, and deleted SIM5-1 and SIM5-2, referred as △SIM5, respectively (Fig. S5G). Co-IP/western blotting results showed that the interaction was efficiently weakened by mSIM2 (^{412}VLDVL^{416}--AAAAA) but not by other mutants of BRCA1 (Fig. 5E).

Since the interaction between PTEN and BRCA1 was dependent on SUMO-SIM, we wondered that the SUMO-site mutant PTEN is also be defective in dephosphorylation of 53BP1. The pT543-53BP1 level was relatively higher in PTEN^{K254R} cells than that in PTEN^{WT} DU145 cells after treatment with Zeocin. However, the pT543-53BP1 level in PTEN^{K266R} cells was comparable with that in PTEN^{WT} cells (Fig. 5F). These suggest that chromatin loading of PTEN mediated by K254-SUMO1 modification is also very important for its role in dephosphorylation of pT543-53BP1. All above results demonstrate that BRCA1 recruits SUMOylated PTEN to chromatin via its N-terminal SIM, thereby dephosphorylating pT543-53BP1 in DDR.

3.6. HR repair is impaired by PTEN^{K254R} *in vivo*

To verify whether SUMO site mutated PTEN impairs HR repair *in vivo*, we generated knock-in mice with a

Fig. 6. HR repair is impaired by PTEN^{K254R} *in vivo*. (A–D) Numbers of 53BP1, γH2AX, RAD51 and RPA32 foci of MEFs post 5 Gy were quantified with FOCO software and presented as dot graph. (E) Immunoblot of pS4/8-RPA32 of MEFs after treatment with 20 Gy. (F) Immunoblot of chromatin loaded PTEN and RPA32 which were separated from MEFs post 20 Gy. (G) Nuclear-cytosol separation of MEFs post 5 Gy and detection of PTEN localization with immunoblot. (H) Immunofluorescence of PTEN in MEFs after 5 Gy treatment and recovery for 4 h. Scale bar, 50 μm. (I) *PtenWT* and *Pten*^{K254R} mice were treated with 8 Gy whole-body IR. Villus length were quantified at indicated time and representative image of HE stained sections of small intestine were shown. More than 100 villi were assessed from each mouse. scale bar, 300 μm. (J) Ki-67 positive cells in intestinal crypts were quantified and representative image of Ki-67 stained sections of small intestine were shown. More than 100 crypts were assessed from each mouse. scale bar, 50 μm. (K) Viability of MEFs treated with Cisplatin, Zeocin or CPT were detected with CCK8 and each group were normalized to no treatment group. Unpaired Student's *t*-test was used (*$P < 0.05$, **$P < 0.01$, ***$P < 0.001$) and data are shown as mean or mean ± SD. All results were shown with one representative image from three independent experiments. Chro., chromatin; CPT, camptothecin; HE, Hematoxylin and Eosin; MEFs, mouse embryonic fibroblasts; NT, non-treatment; WCL, whole cell lysis; WT, wide type.

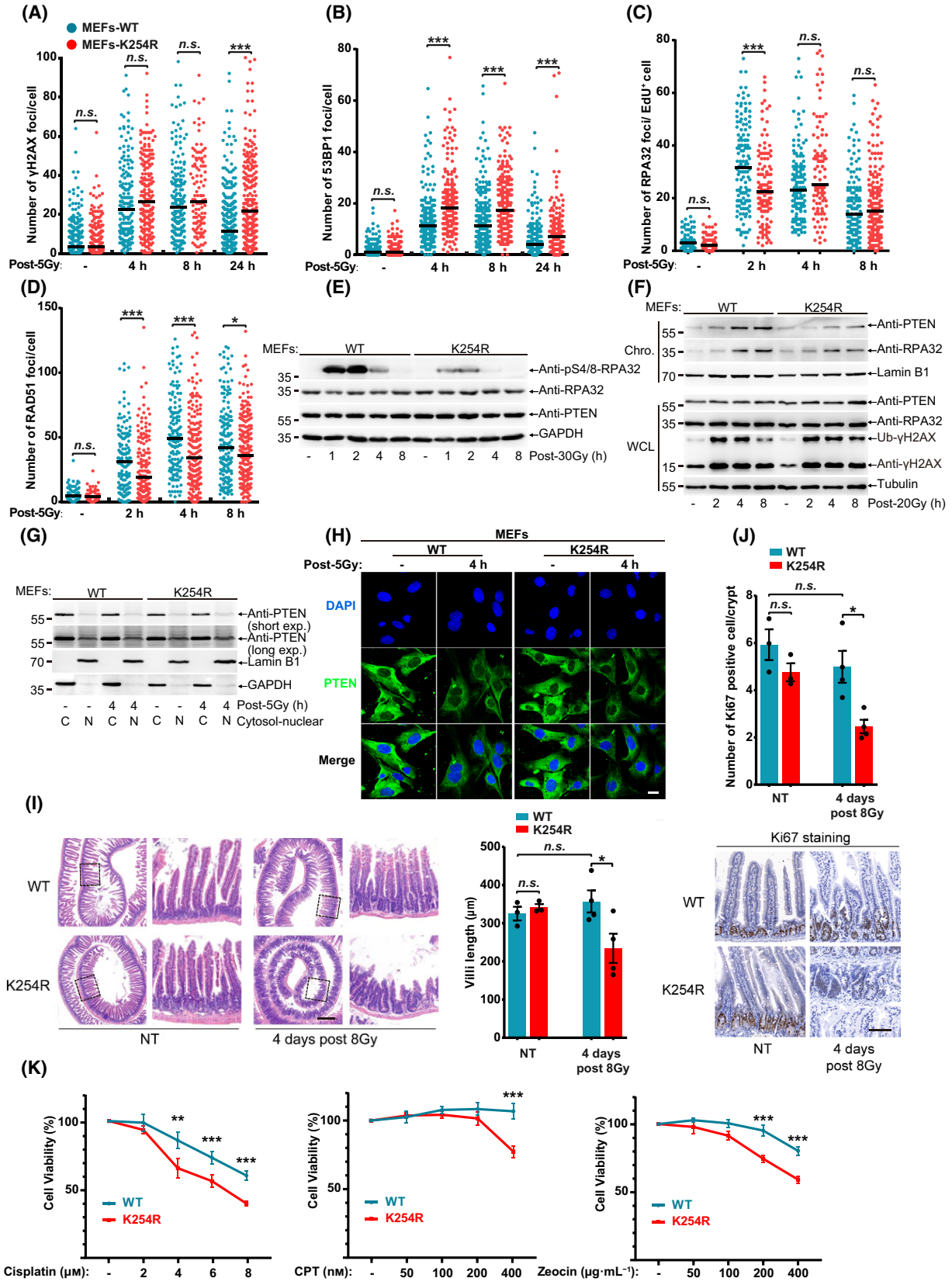
(A)
MEFs-WT
MEFs-K254R
Number of γH2AX foci/cell
Post-5Gy: - 4 h 8 h 24 h
(B)
Number of 53BP1 foci/cell
Post-5Gy: - 4 h 8 h 24 h
(C)
Number of RPA32 foci/ EdU+ cell
Post-5Gy: - 2 h 4 h 8 h
(D)
Number of RAD51 foci/cell
Post-5Gy: - 2 h 4 h 8 h
(E)
MEFs: WT K254R
Anti-pS4/8-RPA32
Anti-RPA32
Anti-PTEN
GAPDH
Post-30Gy (h)
(F)
MEFs: WT K254R
Chro.
WCL
Anti-PTEN
Anti-RPA32
Lamin B1
Ub-γH2AX
Anti-γH2AX
Tubulin
Post-20Gy (h)
(G)
MEFs: WT K254R
Anti-PTEN (short exp.)
Anti-PTEN (long exp.)
Lamin B1
GAPDH
Post-5Gy (h)
Cytosol-nuclear
(H)
MEFs
WT K254R
Post-5Gy: - 4 h - 4 h
DAPI
PTEN
Merge
(J)
WT
K254R
Number of Ki67 positive cell/crypt
NT
4 days post 8Gy
(I)
WT
K254R
NT
4 days post 8Gy
Villi length (μm)
Ki67 staining
(K)
Cell Viability (%)
Cisplatin (μM): - 2 4 6 8
CPT (nM): - 50 100 200 400
Zeocin (μg·mL⁻¹): - 50 100 200 400

point-mutation of *Pten*^{K254R} or *Pten*^{K266R} by using CRISPR-Cas9 technique. *Pten*^{K254R} mice developed normally and was indistinguishable to *Pten*^{WT} mice, but interestingly, *Pten*^{K266R} mice exhibited low birth rate and some of them show abnormal localization of seminal vesicle. Mouse embryonic fibroblasts isolated from *Pten*^{WT} and *Pten*^{K254R} mice were verified by DNA sequencing and used to examine DNA damage repair efficiency (Fig. S6A). Compared with *Pten*^{WT} MEFs, *Pten*^{K254R} MEFs showed significant increase of γH2AX and 53BP1 foci (Fig. 6A,B and Fig. S6B,C) but decrease of RPA32 and RAD51 foci (Fig. 6C,D and Fig. S6D,E) after treatment with IR, indicating *Pten*^{K254R} MEFs were insufficient in HR repair. The levels of γH2AX were also higher in *Pten*^{K254R} MEFs compared to those in *Pten*^{WT} MEFs in the late stage after CPT or Zeocin (Fig. S6F). Furthermore, the pS4/8-RPA32 levels were much weaker in *Pten*^{K254R} MEFs than those in *Pten*^{WT} MEFs after treatment with IR of 20 Gy or 30 Gy (Fig. 6E and Fig. S6G), which proved that PTEN^{K254R} function in regulation of DNA end resection during HR repair was indeed compromised. We also detected pS4/8-RPA32 levels in primary *Pten*^{K254R} MEFs and *Pten*^{WT} MEFs after 30 Gy, and the result was similar with immortalized MEFs (Fig. S6H). Consistent with results of tumor cell lines, PTEN chromatin loading induced by IR and CPT was also inhibited in *Pten*^{K254R} MEFs (Fig. 6F and Fig. S6I). Chromatin-bound RPA32 was also decreased in *Pten*^{K254R} MEFs in response to IR treatment, indicating reduced DNA end resection efficiency (Fig. 6F). Collectively, these data confirm that PTEN^{K254R} impairs HR repair by decreasing its chromatin loading and DNA end resection.

To validate that K254-SUMOylation is essential for PTEN loading to the chromatin to promote HR repair, we isolated the chromatin for analysis of potential PTEN SUMOylation, showing that a shifted 90-kDa which could be SUMOylated PTEN band, was enhanced in *Pten*^{WT} but not in *Pten*^{K254R} MEFs at 4, 8 h after Zeocin treatment (Fig. S6J). One study reported that K254R mutation may affect the subcellular localization of PTEN [18], however our nuclear-cytosol separation results showed there were no any differences between *Pten*^{WT} and *Pten*^{K254R} MEFs under normal condition, even after treatments with IR, CPT or Zeocin (Fig. 6G and Fig. S6K,L). Moreover, immunofluorescence staining of PTEN also displayed not much differences in subcellular localization between *Pten*^{WT} and *Pten*^{K254R} under both normal condition and IR treatment (Fig. 6H). To exclude the impact of cell cycle on DNA damage repair, we also detected the cell cycle profile in primary and immortalized MEFs. There was little differences between *Pten*^{WT} and *Pten*^{K254R} in both primary and immortalized MEFs (Fig. S6M).

To compare the protective effect of *Pten*^{WT} and *Pten*^{K254R} mice against DNA damage under physiological condition, villus length and proliferation of intestinal crypts cells, which are highly sensitive to IR due to their rapid turnover rate [21,34], were determined after treatment with whole-body IR. *Pten*^{WT} mice had no significant difference in crypts morphology and villus length between NT (no treatment) and IR (8 Gy) group, which indicated *Pten*^{WT} mice completely recovered, whereas *Pten*^{K254R} mice showed significant destructed crypts and length-shortened villi 4 days after treatment with IR (Fig. 6I). Similarly, there was no significant difference in numbers of ki67-positive cells between *Pten*^{K254R} and *Pten*^{WT} mice under no treatment, while numbers of ki67-positive cells in intestine crypts of *Pten*^{K254R} mice were less than those of *Pten*^{WT} mice after IR treatment, suggesting reduced proliferating cells of intestine crypts might be due to functional deficiency in DDR (Fig. 6J). These results proved K254-SUMOylation was essential for PTEN mediating DNA damage repair and irradiation protection *in vivo*. Lastly, we tested the sensitivity of *Pten*^{WT} and *Pten*^{K254R} MEFs to DNA damage reagents, and found that *Pten*^{K254R} MEFs were more sensitive to Cisplatin, CPT and Zeocin than *Pten*^{WT} MEFs in a dose-dependent manner (Fig. 6K). Taken together, above results demonstrate that K254-SUMOylation of PTEN is required for PTEN mediating HR repair in DDR *in vivo*.

3.7. Blocking PTEN SUMOylation pathway sensitizes tumor cells to DNA damage reagents

We first determined appropriate concentrations of DNA damage reagents including Cisplatin, Zeocin and CPT for the treatment on DU145-PTEN^{WT} or DU145-PTEN$^{-/-}$ cells, and found that there was little difference in survival colony numbers between DU145-PTEN$^{-/-}$ and DU145-PTEN^{WT} cells when treated with low doses of Cisplatin (0.5 and 1 μM), Zeocin (2 and 5 μg·mL^{-1}) and CPT (25 and 50 nM), whereas DU145-PTEN$^{-/-}$ cells were much more sensitive to high doses of Cisplatin (1.5 and 2 μM), Zeocin (10 and 15 μg·mL^{-1}) and CPT (150 nM) than PTEN^{WT} (Fig. 7A–C and Fig. S7A–C).

Given that SUMOylation signaling is critical for cell survival during DNA damage and a specific SUMO E3 inhibitor is lacking, we tried to assess the cellular sensitivity to DNA damage agents after blocking SUMOylation pathway with SUMO E1 inhibitor,

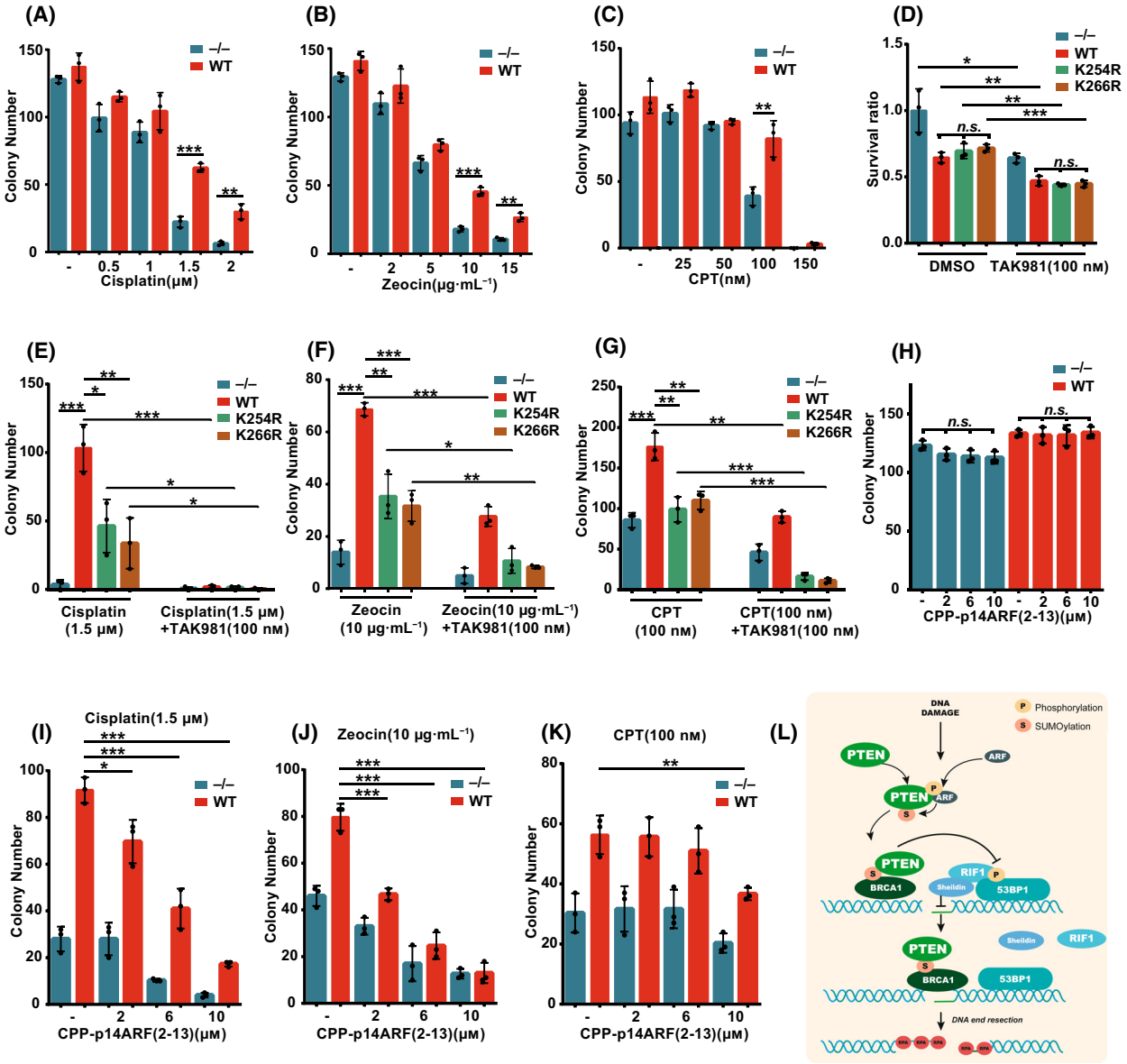

Fig. 7. Blocking PTEN SUMOylation pathway sensitizes tumor cells to DNA damage reagents. (A–C) DU145-PTEN$^{-/-}$ and PTEN^{WT} cells were treated with or without different doses of Cisplatin for 3 days, Zeocin for 2 days or CPT for 2 days and then cultured for another 7–10 days. Colony number was counted and presented as bar graph. (D) DU145-PTEN$^{-/-}$, PTEN^{WT}, PTEN^{K254R} and PTEN^{K266R} cells were treated with or without TAK981 (100 nM) for 3 days and cultured for another 7–10 days. Total intensity of stained colony was measured by IMAGEJ and then normalized to DU145-PTEN$^{-/-}$ group without TAK981 treatment. (E–G) DU145-PTEN$^{-/-}$, PTEN^{WT}, PTEN^{K254R} and PTEN^{K266R} cells were treated with Cisplatin (1.5 μM) for 3 days, Zeocin (10 μg·mL^{-1}) for 2 days or CPT (100 nM) for 2 days or combination with TAK981 (100 nM) and cultured for another 7–10 days. Colony number was counted and presented as bar graph. (H) DU145-PTEN$^{-/-}$ and PTEN^{WT} cells were treated with different doses of CPP-p14ARF(2-13) for 3 days and cultured for another 7–10 days. (I–K) DU145-PTEN$^{-/-}$ and PTEN^{WT} cells were treated with combination of Cisplatin (1.5 μM for 3 days), Zeocin (10 μg·mL^{-1} for 2 days) or CPT (100 nM for 2 days) and different doses of CPP-p14ARF(2-13). Colony number was counted after cultured for another 7–10 days. (L) A schematic model to show the molecular mechanism of PTEN SUMOylation in HR repair. DNA damage induced phosphorylation of p14ARF enhanced its interaction with PTEN and which subsequently promoted SUMOylation of PTEN. SUMOylated PTEN was recognized and recruited into DNA breaks by BRCA1 and then directly dephosphorylated 53BP1 which helped release of its downstream effectors and DNA end resection. 500 cells were seeded in 12-well plates for all colony assays except (C) in which 1000 cells were seeded at the beginning. Unpaired Student's *t*-test was used (*$P < 0.05$, **$P < 0.01$, ***$P < 0.001$) and data are shown as mean ± SD from three biological replicates. All results were shown with one representative image from three independent experiments. CPP-p14ARF(2-13), cell penetrating peptide fused by p14ARF(2-13aa); CPT, camptothecin; WT, wide type.

TAK981 [56], which has been in clinical trial to treat advanced and metastatic solid tumors. In accordance with previous report [57], the total levels of SUMOylation in DU145 cells were inhibited by TAK981 in a dose dependent manner and completely suppressed at the concentration greater than 100 nm (Fig. S7D). We found that TAK981 effectively inhibited the growth/survival of DU145-PTEN$^{-/-}$, -PTEN^{WT}, -PTEN^{K254R} and -PTEN^{K266R} cells, although there was no much difference among PTEN^{WT}, PTEN^{K254R} and PTEN^{K266R} cells either with or without TAK981 treatment (Fig. 7D and Fig. S7E). By assessing combination effects of TAK981 with Cisplatin, Zeocin or CPT, we found that both PTEN^{K254R} and PTEN^{K266R} cells were more sensitive compared with PTEN^{WT} cells (Fig. 7E–G and Fig. S7E), which was consistent with our results that PTEN SUMO site mutations of K254R and K266R decreased DNA damage repair efficiency (Fig. 1C,D). Most strikingly, combination treatment with TAK981 resulted in an additive effect on the sensitivity to Cisplatin, Zeocin or CPT (Fig. 7E–G and Fig. S7E). These results indicated that inhibiting the SUMOylation pathway might increase killing efficiency of DNA damage reagents in clinical cancer treatment.

Since p14ARF knockdown inhibited chromatin loading of PTEN and sensitized DU145 cells to DNA damage (Fig. 3K and Fig. S3H–K), we further synthesized a small peptide called CPP-p14ARF(2-13), which was a Fitc-labeled cell penetrating peptide (CPP) YGRKKR RQRRR fused by p14ARF(2-13aa)/VRRFLVTLRIRR (Fitc-YGRKKRRQRRRVRRFLVTLRIRR), the main region interacting with and promoting PTEN SUMOylation (Fig. 3F). We assessed whether CPP-p14ARF(2-13) can interfere PTEN SUMOylation and loading to the chromatin under DNA damage. Indeed, CPP-p14ARF(2-13) dramatically inhibited the interaction between PTEN and p14ARF (Fig. S7F) as well as chromatin loading of PTEN (Fig. S7G) under CPT treatment. Next, we tested whether CPP-p14ARF(2-13) enhances the cell sensitivity to DNA damage. As previously reported that a peptide of p14ARF(1-22aa) inhibited cell proliferation [58], so we also detected whether CPP-p14ARF(2-13) influences it. There was no difference in survival colony numbers between PTEN$^{-/-}$ and PTEN^{WT} DU145 cells treated with CPP-p14ARF(2-13) in different doses, suggesting CPP-p14ARF(2-13) did not affect cell proliferation (Fig. 7H and Fig. S7H). Interestingly, the cell sensitivity to Cisplatin, Zeocin or CPT treatment was increased by combination with CPP-p14ARF(2-13) (Fig. 7I–K and Fig. S7H). The low dose of CPP-p14ARF(2-13) at 2 μM was capable to enhance killing efficiency for Cisplatin and Zeocin treatments to DU145-PTEN^{WT} cells (Fig. 7I,J), and the high dose at 10 μM also increased killing efficiency for CPT treatment (Fig. 7K). Furthermore, CPP-p14ARF (2-13) treatment also decreased survival rate of DU145-PTEN$^{-/-}$ cells when combined with these reagents, suggesting CPP-p14ARF(2-13) might block the interaction of p14ARF with other targets besides PTEN. Thus, above results suggest that TAK981 or CPP-p14ARF(2-13) has the potential to enhance the effect of DNA damage reagents in killing tumor cells.

4. Discussion

Post-translational modifications of PTEN including SUMOylation [18], methylation and phosphorylation [24] are involved in DDR. Although one study reported that PTEN^{K254R} impaired HR repair efficiency, the underlying molecular mechanism remained largely elusive [18]. Our data suggested that DNA damage induced PTEN SUMOylation in a time-dependent manner other than rapid activation like phosphorylation. Both K254 and K266 of PTEN could be conjugated with SUMO1, but one single mutation was enough to reduce DNA damage-induced PTEN SUMOylation. Interestingly, the mutation K254R, but not K266R, suppressed DNA damage-triggered PTEN chromatin loading. It is an open question how K266-SUMOylation of PTEN to participate in DDR. Given that K266 has also been identified as a ubiquitination site [59], it might exist a crosstalk between SUMOylation and ubiquitination of PTEN during DDR. Moreover, SUMOylation of PTEN on K266 promotes its association with cell membrane and which in turn inhibits PI3K-AKT signaling [25]. As PI3K-AKT pathway can be also activated by DNA damage stimuli and regulated function of DDR related proteins [60–63], K266-SUMOylation of PTEN might also promote DDR through the PI3K-AKT pathway. Additionally, the mutation C124S remarkably enhanced PTEN nuclear localization and chromatin loading. Due to PTEN interacting with RAD51 and RPA32 [19,23], this might explain why PTEN^{C124S} decreased HR repair efficiency but not affected the chromatin loading of RAD51 and RPA32. It remains to be further explored how C124S influences PTEN localization and whether the chromatin trapped PTEN^{C124S} has other additive side effects on DNA damage repair.

Several SUMO E3 ligases including PIAS1, PIAS4, CBX4 and ZNF451 play an important role in regulation of SUMOylation signal transduction in response to DNA damage [32,33,64]. Here, we identified an atypical SUMO E3 ligase, p14ARF, responsible for

PTEN SUMOylation under DNA damage such as IR, CPT and Zeocin through their interaction, which was enhanced by DNA damage-induced phosphorylation of p14ARF. UV stress disrupts the p14ARF-B23 interaction in the nucleolar, resulting in a transient translocation of p14ARF to the nucleoplasm [65]. In addition, ATM, a main DDR kinase, promotes the release of p14ARF from the nucleus and subsequent degradation after doxorubicin treatment [66]. So, the sub-nuclear distribution and protein–protein interactions of p14ARF are critical for its function in promoting PTEN SUMOylation after DNA damage.

As for the role of PTEN protein phosphatase in HR repair, the conclusions from two different groups are contradictory [21,24]. Our results supported that PTEN protein phosphatase was necessary for HR repair. In addition to γH2AX as a substrate of PTEN during DDR [24], we identified a new target, 53BP1, which was directly dephosphorylated by PTEN in cells and *in vitro*. More interestingly, PTEN selectively dephosphorylated pT543-53BP1 other than pS25-53BP1 in cells. It has been early reported that phosphorylation at 7S/TQ sites in the N-terminal region of 53BP1 is responsible for its recruitment of RIF1, whereas phosphorylation at the other 8S/TQ sites of 53BP1 is essential for PTIP accumulation at DNA-break sites [7]. And interestingly, as long as one site of 7S/TQ is phosphorylated, it is sufficient for 53BP1 recruiting RIF1 [14]. However, most recently one study reported that RIF1 is recruited to IR-induced foci by recognizing three related phosphorylated epitopes on 53BP1 [67]. Thus, PTEN might also target phosphorylation at other sites responsible for RIF1 recruitment, besides pT543-53BP1 that is one of 7S/TQ, during DDR. In addition, it has been reported another phosphatase, PP4C, dephosphorylates 53BP1 and promotes HR repair [14]. Given that knockout of PP4C or PTEN can upregulate the phosphorylation of 53BP1, both PP4C and PTEN are probably necessary rather than redundant for inhibiting the phosphorylation of 53BP1. However, it is not yet clear whether the function of PP4C or PTEN is specific to cell type or DNA damage. More efforts are needed to further differentiate their roles in this process.

As known that BRCA1 is critical for HR repair by against 53BP1 posted barrier through serval molecular mechanisms, including inhibition of 53BP1 phosphorylation [14]. Our results supported that PTEN was a downstream effector of BRCA1 and PTEN SUMOylation was required for their interaction, which was efficiently decreased by double mutation of K254/266R. One SIM located in the N terminus of BRCA1 was essential for recognition of SUMO1 conjugated to PTEN, by which PTEN was subsequently recruited by BRCA1 to DNA-break sites. This might partially explain why that the deletion of *exon11* of BRCA1 resulted in loss of BRCA1 function in inhibition of phosphorylation of 53BP1 [15,16].Moreover, as 53BP1 is pro-choice for DNA breaks and BRCA1 complex can relocate into the core of 53BP1 foci at S/G2 in a time dependent manner [68,69], so we speculate that after entering the core, BRCA1 recruits PTEN to directly dephosphorylate 53BP1, thus releasing downstream effectors of 53BP1 such as RIF1 and PTIP, which further facilitates DNA end resection and ongoing of HR repair.

The *in vivo* results from $Pten^{K254R}$ mice validated that PTEN SUMOylation promoted HR repair. Significantly, we did not observe the mutation K254R influence PTEN nuclear localization [18], by *in vivo* and *in vitro* results, which is consistent with our early report [25]. However, our data strongly demonstrated that SUMOylation of PTEN was induced by several DNA damage agents and this sub-pool of SUMOylated PTEN was tightly associated with chromatin via BRCA1. It is worth noting that Bassi et al. [18] claimed that K254-SUMOylated-PTEN was decreased and excluded from the nucleus upon DNA damage, which was totally inconsistent with our observations that SUMO-mutant K254R had no differences in the localization. We have analyzed the possible reasons for these discrepancies as follows. Firstly, in addition to our model, several studies have reported that PTEN nuclear localization or chromatin association is important for DNA damage repair. For examples, Hou et al. [70] showed that Grb2 mediates PTEN nuclear translocation to repair H_2O_2-induced DNA damage in HeLa cells. Chen et al. [71] found that the activation of ATM by DNA damage reagents phosphorylates PTEN at Ser113, which promotes PTEN nuclear retention in HeLa and A549 cells. Ma et al. [21] found that FGFR phosphorylates PTEN at Y240 to facilitate PTEN nuclear localization and recruitment onto chromatin after IR treatment. Zhang et al. [24] also presented evidences that the phosphorylation at T398 of PTEN induced by DNA damage is recognized by MCD1 to promote PTEN chromatin loading. All above studies suggest that PTEN nuclear localization or chromatin association is a prerequisite to perform its function during DNA damage repair. However, Bassi et al. showed that re-expressed PTEN in U87MG, which is a PTEN-deficient gliomas cell line, was excluded from the nucleus after IR treatment. This was inconsistent with our observation in DU145 that is a prostate cancer cell line with the expression of endogenous PTEN. We guess the exclusion of exogenous PTEN in U87MG cells after IR might be a cell

type-specific phenotype. Second, Bassi et al. also claimed that SUMOylated-PTEN, which was mostly localized in the nucleus in basal conditions, was excluded from the nucleus after DNA damage. They conducted the nuclear-cytosol fractionation to detect endogenous PTEN in HeLa cells after IR treatment and found that the nuclear PTEN was significantly decreased. It was very interesting that two close bands higher than normal PTEN were observed, which they thought as SUMOylated PTEN. However, these two bands are more likely to be the other two isoforms, PTENα and PTENβ [72], which are both recently discovered. Third, for the nuclear-cytosol separation assay, nuclear fraction consists of both soluble and precipitated parts. Soluble part contains soluble proteins, while precipitated part is mainly made up of chromatin and its associated proteins. Detailed nuclear-cytosol separation method was not included in their paper. In our results, SUMOylated PTEN was tightly bound with chromatin and mainly in the nuclear precipitates during DNA damage repair. Therefore, another possible explanation is that they might detected only soluble part of nuclear fractions but not whole or precipitated fractions, which resulted in decreased level of SUMOylated PTEN in their observation. In all, the discrepancies between these results needs to be further explored. More efforts should be made to analyze the SUMOylation of PTEN at K254 in different cellular context during DNA damage repair.

Since we proved that activation of SUMOylation pathway was essential for correct DNA damage repair, so the combination of SUMOylation inhibitor with DNA damage reagents might enhance sensitivity of tumor cells to chemotherapy. As expectedly, the SUMOylation inhibitor TAK981 remarkedly increased killing efficiency of DNA damage reagents. Furthermore, the small peptide CPP-p14ARF(2-13) also suppressed DNA damage-induced chromatin loading of PTEN and sensitized tumor cells to chemotherapy.

5. Conclusions

In summary, our study uncovers a new mechanism that SUMOylated PTEN promotes HR repair through dephosphorylation of 53BP1 (Fig. 7L). In response to DNA damage, p14ARF as a SUMO E3 ligase is phosphorylated to enhance the interaction with PTEN in the nucleus, which subsequently promotes PTEN SUMOylation. Then, SUMOylated PTEN is recognized and recruited to the chromatin near DSB by the N-terminal SIM of BRCA1. This pool of PTEN relieves HR repair barrier posted by 53BP1 through directly dephosphorylating 53BP1, promoting HR repair. Blocking PTEN SUMOylation pathway by TAK981 and CPP-p14ARF(2-13) sensitizes tumor cells to DNA damage reagents. Thus, our study elucidated a new molecular mechanism of the key role of PTEN in HR repair during DDR, which may provide a new strategy for clinical cancer therapy.

Acknowledgements

This work was supported by grants from China's National Key R&D Programmes (NKP) (No. 2019YFE0110600), the National Natural Science Foundation of China (82230100, 81630075, 32271310, 82103082, 81721004), and Shanghai Science and Technology Commission (20JC1410100).

Conflict of interest

The authors declare no conflict of interest.

Author contributions

JY, JHe, and RD conceived and designed the study. JHu, YG, and RD performed most of the experiments. CH performed all those revised experiments. LL, RC, YW, XZ, JHu, and JZ helped with experiments and provided technical support. JY, JHe, YG, and RD analyzed the data. JY, JHe, and XZ wrote the manuscript. All authors read and approved the final manuscript.

Peer review

The peer review history for this article is available at https://www.webofscience.com/api/gateway/wos/peer-review/10.1002/1878-0261.13563.

Data availability statement

The datasets used and/or analyzed during this study are available from the corresponding author upon reasonable request.

References

1 Roos WP, Thomas AD, Kaina B. DNA damage and the balance between survival and death in cancer biology. *Nat Rev Cancer*. 2016;**16**:20–33. https://doi.org/10.1038/nrc.2015.2

2 Tubbs A, Nussenzweig A. Endogenous DNA damage as a source of genomic instability in cancer. *Cell*. 2017;**168**:644–56. https://doi.org/10.1016/j.cell.2017.01.002

3 Chen JY, Li P, Song LC, Bai L, Huen MSY, Liu YD, et al. 53BP1 loss rescues embryonic lethality but not genomic instability of BRCA1 total knockout mice. *Cell Death Differ*. 2020;**27**:2552–67. https://doi.org/10.1038/s41418-020-0521-4
4 Lord CJ, Ashworth A. BRCAness revisited. *Nat Rev Cancer*. 2016;**16**:110–20. https://doi.org/10.1038/nrc.2015.21
5 Scully R, Panday A, Elango R, Willis NA. DNA double-strand break repair-pathway choice in somatic mammalian cells. *Nat Rev Mol Cell Biol*. 2019;**20**:698–714. https://doi.org/10.1038/s41580-019-0152-0
6 Panier S, Boulton SJ. Double-strand break repair: 53BP1 comes into focus. *Nat Rev Mol Cell Biol*. 2014;**15**:7–18. https://doi.org/10.1038/nrm3719
7 Callen E, Di Virgilio M, Kruhlak MJ, Nieto-Soler M, Wong N, Chen HT, et al. 53BP1 mediates productive and mutagenic DNA repair through distinct phosphoprotein interactions. *Cell*. 2013;**153**:1266–80. https://doi.org/10.1016/j.cell.2013.05.023
8 Gupta R, Somyajit K, Narita T, Maskey E, Stanlie A, Kremer M, et al. DNA repair network analysis reveals Shieldin as a key regulator of NHEJ and PARP inhibitor sensitivity. *Cell*. 2018;**173**:972–88. https://doi.org/10.1016/j.cell.2018.03.050
9 Noordermeer SM, Adam S, Setiaputra D, Barazas M, Pettitt SJ, Ling AK, et al. The shieldin complex mediates 53BP1-dependent DNA repair. *Nature*. 2018;**560**:117–21. https://doi.org/10.1038/s41586-018-0340-7
10 Zimmermann M, Lottersberger F, Buonomo SB, Sfeir A, de Lange T. 53BP1 regulates DSB repair using Rif1 to control 5′ end resection. *Science*. 2013;**339**:700–4. https://doi.org/10.1126/science.1231573
11 Chapman JR, Taylor MRG, Boulton SJ. Playing the end game: DNA double-Strand break repair pathway choice. *Mol Cell*. 2012;**47**:497–510. https://doi.org/10.1016/j.molcel.2012.07.029
12 Huen MSY, Sy SMH, Chen JJ. BRCA1 and its toolbox for the maintenance of genome integrity. *Nat Rev Mol Cell Biol*. 2010;**11**:138–48. https://doi.org/10.1038/nrm2831
13 Zhang HX, Liu HL, Chen YL, Yang X, Wang PF, Liu TZ, et al. A cell cycle-dependent BRCA1-UHRF1 cascade regulates DNA double-strand break repair pathway choice. *Nat Commun*. 2016;**7**:10201. https://doi.org/10.1038/ncomms10201
14 Isono M, Niimi A, Oike T, Hagiwara Y, Sato H, Sekine R, et al. BRCA1 directs the repair pathway to homologous recombination by promoting 53BP1 Dephosphorylation. *Cell Rep*. 2017;**18**:520–32. https://doi.org/10.1016/j.celrep.2016.12.042
15 Nacson J, Di Marcantonio D, Wang YF, Bernhardy AJ, Clausen E, Hua X, et al. BRCA1 mutational complementation induces synthetic viability. *Mol Cell*. 2020;**78**:951–9. https://doi.org/10.1016/j.molcel.2020.04.006
16 Nacson J, Krais JJ, Bernhardy AJ, Clausen E, Feng WJ, Wang YF, et al. BRCA1 mutation-specific responses to 53BP1 loss-induced homologous recombination and PARP inhibitor resistance (vol 24, 3513, 2018). *Cell Rep*. 2018;**25**:1384. https://doi.org/10.1016/j.celrep.2018.10.009
17 Lee YR, Chen M, Pandolfi PP. The functions and regulation of the PTEN tumour suppressor: new modes and prospects. *Nat Rev Mol Cell Biol*. 2018;**19**:547–62. https://doi.org/10.1038/s41580-018-0015-0
18 Bassi C, Ho J, Srikumar T, Dowling RJ, Gorrini C, Miller SJ, et al. Nuclear PTEN controls DNA repair and sensitivity to genotoxic stress. *Science*. 2013;**341**:395–9. https://doi.org/10.1126/science.1236188
19 He JX, Kang X, Yin YX, Chao KSC, Shen WH. PTEN regulates DNA replication progression and stalled fork recovery. *Nat Commun*. 2015;**6**:7620. https://doi.org/10.1038/ncomms8620
20 Ho J, Cruise ES, Dowling RJO, Stambolic V. PTEN nuclear functions. *Cold Spring Harb Perspect Med*. 2020;**10**:a036079. https://doi.org/10.1101/cshperspect.a036079
21 Ma J, Benitez JA, Li J, Miki S, Ponte de Albuquerque C, Galatro T, et al. Inhibition of nuclear PTEN tyrosine phosphorylation enhances glioma radiation sensitivity through attenuated DNA repair. *Cancer Cell*. 2019;**36**:690–1. https://doi.org/10.1016/j.ccell.2019.11.008
22 Shen WH, Balajee AS, Wang J, Wu H, Eng C, Pandolfi PP, et al. Essential role for nuclear PTEN in maintaining chromosomal integrity. *Cell*. 2007;**128**:157–70. https://doi.org/10.1016/j.cell.2006.11.042
23 Wang GX, Li Y, Wang P, Liang H, Cui M, Zhu ML, et al. PTEN regulates RPA1 and protects DNA replication forks. *Cell Res*. 2015;**25**:1189–204. https://doi.org/10.1038/cr.2015.115
24 Zhang J, Lee YR, Dang F, Gan W, Menon AV, Katon JM, et al. PTEN methylation by NSD2 controls cellular sensitivity to DNA damage. *Cancer Discov*. 2019;**9**:1306–23. https://doi.org/10.1158/2159-8290.CD-18-0083
25 Huang J, Yan J, Zhang J, Zhu S, Wang Y, Shi T, et al. SUMO1 modification of PTEN regulates tumorigenesis by controlling its association with the plasma membrane. *Nat Commun*. 2012;**3**:911. https://doi.org/10.1038/ncomms1919
26 Dhingra N, Zhao XL. Intricate SUMO-based control of the homologous recombination machinery. *Genes Dev*. 2019;**33**:1346–54. https://doi.org/10.1101/gad.328534
27 Schwertman P, Bekker-Jensen S, Mailand N. Regulation of DNA double-strand break repair by ubiquitin and ubiquitin-like modifiers. *Nat Rev Mol*

Cell Biol. 2016;**17**:379–94. https://doi.org/10.1038/nrm.2016.58

28 Choi BH, Chen Y, Dai W. Chromatin PTEN is involved in DNA damage response partly through regulating Rad52 sumoylation. *Cell Cycle*. 2013;**12**:3442–7. https://doi.org/10.4161/cc.26465

29 Cremona CA, Sarangi P, Yang Y, Hang LE, Rahman S, Zhao X. Extensive DNA damage-induced sumoylation contributes to replication and repair and acts in addition to the mec1 checkpoint. *Mol Cell*. 2012;**45**:422–32. https://doi.org/10.1016/j.molcel.2011.11.028

30 Ismail IH, Gagne JP, Caron MC, McDonald D, Xu Z, Masson JY, et al. CBX4-mediated SUMO modification regulates BMI1 recruitment at sites of DNA damage. *Nucleic Acids Res*. 2012;**40**:5497–510. https://doi.org/10.1093/nar/gks222

31 Ouyang KJ, Woo LL, Zhu J, Huo D, Matunis MJ, Ellis NA. SUMO modification regulates BLM and RAD51 interaction at damaged replication forks. *PLoS Biol*. 2009;**7**:e1000252. https://doi.org/10.1371/journal.pbio.1000252

32 Soria-Bretones I, Cepeda-Garcia C, Checa-Rodriguez C, Heyer V, Reina-San-Martin B, Soutoglou E, et al. DNA end resection requires constitutive sumoylation of CtIP by CBX4. *Nat Commun*. 2017;**8**:113. https://doi.org/10.1038/s41467-017-00183-6

33 Tian T, Bu M, Chen X, Ding LL, Yang YL, Han JH, et al. The ZATT-TOP2A-PICH Axis drives extensive replication fork reversal to promote genome stability. *Mol Cell*. 2021;**81**:198–211. https://doi.org/10.1016/j.molcel.2020.11.007

34 Xie X, Hu H, Tong X, Li L, Liu X, Chen M, et al. The mTOR-S6K pathway links growth signalling to DNA damage response by targeting RNF168. *Nat Cell Biol*. 2018;**20**:320–31. https://doi.org/10.1038/s41556-017-0033-8

35 Ha K, Ma C, Lin H, Tang L, Lian Z, Zhao F, et al. The anaphase promoting complex impacts repair choice by protecting ubiquitin signalling at DNA damage sites. *Nat Commun*. 2017;**8**:15751. https://doi.org/10.1038/ncomms15751

36 Peng B, Wang J, Hu Y, Zhao H, Hou W, Zhao H, et al. Modulation of LSD1 phosphorylation by CK2/WIP1 regulates RNF168-dependent 53BP1 recruitment in response to DNA damage. *Nucleic Acids Res*. 2015;**43**:5936–47. https://doi.org/10.1093/nar/gkv528

37 Yu JX, Zhang SS, Saito K, Williams S, Arimura Y, Ma YL, et al. PTEN regulation by Akt-EGR1-ARF-PTEN axis. *EMBO J*. 2009;**28**:21–33. https://doi.org/10.1038/emboj.2008.238

38 Lapytsko A, Kollarovic G, Ivanova L, Studencka M, Schaber J. FoCo: a simple and robust quantification algorithm of nuclear foci. *BMC Bioinformatics*. 2015;**16**:392. https://doi.org/10.1186/s12859-015-0816-5

39 Bjergbæk L. DNA repair protocols. 3rd ed. New York: Humana Press/Springer; 2012.

40 Mendez J, Stillman B. Chromatin association of human origin recognition complex, Cdc6, and minichromosome maintenance proteins during the cell cycle: assembly of prereplication complexes in late mitosis. *Mol Cell Biol*. 2000;**20**:8602–12. https://doi.org/10.1128/Mcb.20.22.8602–8612.2000

41 Symington LS. Mechanism and regulation of DNA end resection in eukaryotes. *Crit Rev Biochem Mol Biol*. 2016;**51**:195–212. https://doi.org/10.3109/10409238.2016.1172552

42 Wu X, Wang B. Abraxas suppresses DNA end resection and limits break-induced replication by controlling SLX4/MUS81 chromatin loading in response to TOP1 inhibitor-induced DNA damage. *Nat Commun*. 2021;**12**:4373. https://doi.org/10.1038/s41467-021-24665-w

43 Andegeko Y, Moyal L, Mittelman L, Tsarfaty I, Shiloh Y. Rotman G nuclear retention of ATM at sites of DNA double strand breaks. *J Biol Chem*. 2001;**276**:38224–30.

44 Yang QY, Zhu Q, Lu XP, Du YP, Cao LL, Shen CC, et al. G9a coordinates with the RPA complex to promote DNA damage repair and cell survival. *Proc Natl Acad Sci USA*. 2017;**114**:E6054–63. https://doi.org/10.1073/pnas.1700694114

45 Weinstock DM, Nakanishi K, Helgadottir HR, Jasin M. Assaying double-strand break repair pathway choice in mammalian cells using a targeted endonuclease or the RAG recombinase. *Methods Enzymol*. 2006;**409**:524–40. https://doi.org/10.1016/S0076-6879(05)09031-2

46 Ozenne P, Eymin B, Brambilla E, Gazzeri S. The ARF tumor suppressor: structure, functions and status in cancer. *Int J Cancer*. 2010;**127**:2239–47. https://doi.org/10.1002/ijc.25511

47 Tago K, Chiocca S, Sherr CJ. Sumoylation induced by the Arf tumor suppressor: a p53-independent function. *Proc Natl Acad Sci USA*. 2005;**102**:7689–94. https://doi.org/10.1073/pnas.0502978102

48 Woods YL, Xirodimas DP, Prescott AR, Sparks A, Lane DP, Saville MK. p14 Arf promotes small ubiquitin-like modifier conjugation of Werners helicase. *J Biol Chem*. 2004;**279**:50157–66. https://doi.org/10.1074/jbc.M405414200

49 Fontana R, Guidone D, Sangermano F, Calabro V, Pollice A, La Mantia G, et al. PKC dependent p14ARF phosphorylation on threonine 8 drives cell proliferation. *Sci Rep*. 2018;**8**:7056. https://doi.org/10.1038/s41598-018-25496-4

50 Callen E, Zong DL, Wu W, Wong N, Stanlie A, Ishikawa M, et al. 53BP1 enforces distinct pre- and post-resection blocks on homologous recombination. *Mol Cell*. 2020;**77**:26–38. https://doi.org/10.1016/j.molcel.2019.09.024

51 Feng L, Fong KW, Wang JD, Wang WQ, Chen JJ. RIF1 counteracts BRCA1-mediated end resection during DNA repair. *J Biol Chem*. 2013;**288**:11135–43. https://doi.org/10.1074/jbc.M113.457440
52 Mirman Z, Lottersberger F, Takai H, Kibe T, Gong Y, Takai K, et al. 53BP1-RIF1-shieldin counteracts DSB resection through CST- and pol alpha-dependent fill-in. *Nature*. 2018;**560**:112–6. https://doi.org/10.1038/s41586-018-0324-7
53 Chia JY, Gajewski JE, Xiao Y, Zhu HJ, Cheng HC. Unique biochemical properties of the protein tyrosine phosphatase activity of PTEN-demonstration of different active site structural requirements for phosphopeptide and phospholipid phosphatase activities of PTEN. *Biochim Biophys Acta*. 2010;**1804**:1785–95. https://doi.org/10.1016/j.bbapap.2010.05.009
54 Beauclair G, Bridier-Nahmias A, Zagury JF, Saib A, Zamborlini A. JASSA: a comprehensive tool for prediction of SUMOylation sites and SIMs. *Bioinformatics*. 2015;**31**:3483–91. https://doi.org/10.1093/bioinformatics/btv403
55 Zhao Q, Xie Y, Zheng Y, Jiang S, Liu W, Mu W, et al. GPS-SUMO: a tool for the prediction of sumoylation sites and SUMO-interaction motifs. *Nucleic Acids Res*. 2014;**42**:W325–30. https://doi.org/10.1093/nar/gku383
56 Langston SP, Grossman S, England D, Afroze R, Bence N, Bowman D, et al. Discovery of TAK-981, a first-in-class inhibitor of SUMO-activating enzyme for the treatment of cancer. *J Med Chem*. 2021;**64**:2501–20. https://doi.org/10.1021/acs.jmedchem.0c01491
57 Lightcap ES, Yu P, Grossman S, Song K, Khattar M, Xega K, et al. A small-molecule SUMOylation inhibitor activates antitumor immune responses and potentiates immune therapies in preclinical models. *Sci Transl Med*. 2021;**13**:eaba7791. https://doi.org/10.1126/scitranslmed.aba7791
58 Johansson HJ, El-Andaloussi S, Holm T, Mae M, Janes J, Maimets T, et al. Characterization of a novel cytotoxic cell-penetrating peptide derived from p14ARF protein. *Mol Ther*. 2008;**16**:115–23. https://doi.org/10.1038/sj.mt.6300346
59 He YM, Zhou XM, Jiang SY, Zhang ZB, Cao BY, Liu JB, et al. TRIM25 activates AKT/mTOR by inhibiting PTEN via K63-linked polyubiquitination in non-small cell lung cancer. *Acta Pharmacol Sin*. 2021;**43**:681–91. https://doi.org/10.1038/s41401-021-00662-z
60 Golding SE, Morgan RN, Adams BR, Hawkins AJ, Povirk LF, Valerie K. Pro-survival AKT and ERK signaling from EGFR and mutant EGFRvIII enhances DNA double-strand break repair in human glioma cells. *Cancer Biol Ther*. 2009;**8**:730–8. https://doi.org/10.4161/cbt.8.8.7927
61 Hu L, Li X, Liu Q, Xu J, Ge H, Wang Z, et al. UBE2S, a novel substrate of Akt1, associates with Ku70 and regulates DNA repair and glioblastoma multiforme resistance to chemotherapy. *Oncogene*. 2017;**36**:1145–56. https://doi.org/10.1038/onc.2016.281
62 Jia Y, Song W, Zhang F, Yan J, Yang Q. Akt1 inhibits homologous recombination in Brca1-deficient cells by blocking the Chk1-Rad51 pathway. *Oncogene*. 2013;**32**:1943–9. https://doi.org/10.1038/onc.2012.211
63 Plo I, Laulier C, Gauthier L, Lebrun F, Calvo F, Lopez BS. AKT1 inhibits homologous recombination by inducing cytoplasmic retention of BRCA1 and RAD51. *Cancer Res*. 2008;**68**:9404–12. https://doi.org/10.1158/0008-5472.CAN-08-0861
64 Galanty Y, Belotserkovskaya R, Coates J, Polo S, Miller KM, Jackson SP. Mammalian SUMO E3-ligases PIAS1 and PIAS4 promote responses to DNA double-strand breaks. *Nature*. 2009;**462**:935–9. https://doi.org/10.1038/nature08657
65 Lee C, Smith BA, Bandyopadhyay K, Gjerset RA. DNA damage disrupts the p14ARF-B23 (nucleophosmin) interaction and triggers a transient subnuclear redistribution of p14ARF. *Cancer Res*. 2005;**65**:9834–42. https://doi.org/10.1158/0008-5472.CAN-05-1759
66 Velimezi G, Liontos M, Vougas K, Roumeliotis T, Bartkova J, Sideridou M, et al. Functional interplay between the DNA-damage-response kinase ATM and ARF tumour suppressor protein in human cancer. *Nat Cell Biol*. 2013;**15**:967–77. https://doi.org/10.1038/ncb2795
67 Setiaputra D, Escribano-Diaz C, Reinert JK, Sadana P, Zong D, Callen E, et al. RIF1 acts in DNA repair through phosphopeptide recognition of 53BP1. *Mol Cell*. 2022;**82**:1359–1371 e1359. https://doi.org/10.1016/j.molcel.2022.01.025
68 Chapman JR, Sossick AJ, Boulton SJ, Jackson SP. BRCA1-associated exclusion of 53BP1 from DNA damage sites underlies temporal control of DNA repair. *J Cell Sci*. 2012;**125**:3529–34. https://doi.org/10.1242/jcs.105353
69 Zimmermann M, de Lange T. 53BP1: pro choice in DNA repair. *Trends Cell Biol*. 2014;**24**:108–17. https://doi.org/10.1016/j.tcb.2013.09.003
70 Hou BL, Xu SS, Xu Y, Gao Q, Zhang CN, Liu L, et al. Grb2 binds to PTEN and regulates its nuclear translocation to maintain the genomic stability in DNA damage response. *Cell Death Dis*. 2019;**10**:546. https://doi.org/10.1038/s41419-019-1762-3
71 Chen JH, Zhang P, Chen WD, Li DD, Wu XQ, Deng R, et al. ATM-mediated PTEN phosphorylation promotes PTEN nuclear translocation and autophagy in response to DNA-damaging agents in cancer cells. *Autophagy*. 2015;**11**:239–52. https://doi.org/10.1080/15548627.2015.1009767

72 Shen SM, Zhang C, Ge MK, Dong SS, Xia L, He P, et al. PTENalpha and PTENbeta promote carcinogenesis through WDR5 and H3K4 trimethylation. *Nat Cell Biol*. 2019;**21**:1436–48. https://doi.org/10.1038/s41556-019-0409-z

Supporting information

Additional supporting information may be found online in the Supporting Information section at the end of the article.

Fig. S1. PTEN promotes HR repair through enhancing DNA end resection.

Fig. S2. DNA damage promotes PTEN chromatin loading by inducing its SUMOylation.

Fig. S3. p14ARF is a novel SUMO E3 ligase to mediate PTEN SUMOylation during DDR.

Fig. S4. PTEN relieves HR barrier posted by 53BP1 through directly dephosphorylating pT543-53BP1.

Fig. S5. PTEN chromatin loading is mediated by BRCA1 recruiting SUMOylated PTEN via its N-terminal SIM.

Fig. S6. Homologous recombination repair is impaired by SUMO-deficient PTEN *in vivo*.

Fig. S7. Blocking PTEN SUMOylation pathway sensitizes tumor cells to DNA damage reagents.

Table S1. List of antibodies used in this study.

Table S2. Sequences of shRNA, siRNA, and sgRNA used in this study.